LITHOGRAPHIC RESISTS

1. Introduction

Lithography in its original meaning describes a method of printing where a master pattern or design is formed first on a stone or metal surface using a hydrophobic material, the pattern is wetted with a hydrophobic ink, and finally the inked pattern is transferred to paper to produce copies of the master. Today, the meaning of the term has broadened to include a number of methods for replicating a predetermined pattern on a substrate, for an increasing variety of purposes. In most cases, replication is effected by first coating the substrate with a photosensitive polymer film termed a *lithographic resist*, and then exposing the film to a pattern of light . Photochemically induced changes in areas of the film exposed to light alter solubility to such an extent that either exposed or unexposed areas can be selectively dissolved to reveal portions of the substrate surface. If the exposed areas of resist become insoluble, then the resist is termed negative acting; if solubility of the exposed regions increases, then the resist is termed positive acting.

In certain applications, the resist film becomes a permanent, functional component of the device being constructed, typically serving as an electrical insulator or protective encapsulant. In such cases, the patterned film often is treated to enhance chemical resistance and mechanical properties . Most commonly, however, the resist pattern is a temporary template, and is removed or stripped after the image has been transferred to the substrate. Numerous methods of image transfer have been practiced, including plating and deposition (*additive* processing), chemical etching or physical milling to erode the exposed substrate (*subtractive* processing), or bombardment with energetic ions that become implanted in the substrate surface. Figure summarizes the steps comprising the lithographic process.

Lithographic resists enable a host of technological advances that have had far-ranging impacts. For example, the rapid progress in microelectronics technology in large part stems from refinement of the lithographic techniques used to fabricate computer integrated circuits. The ability to pack ever-increasing numbers of discrete electronic components in a given area of an integrated circuit, when coupled with the economies of scale that result from high volume manufacturing, has led to both improved performance and lower cost with each succeeding generation . Today, in 2005, the annual global market for semiconductors far exceeds $200 billion.

The advantages of miniaturization are now being exploited in areas beyond microelectronics. Adaptation of materials and processes originally devised for semiconductor manufacture has allowed fabrication of sensors (eg, pressure meters and accelerometers used in the automotive industry) , complex optical , and micromechanical assemblies, and devices for medical diagnostics using lithographic resists.

2. Essential Attributes of Lithographic Resists

Regardless of the specific application, all resists must display certain fundamental functional properties:

- The resist composition must form *uniform, defect-free films* on the substrate of interest. To achieve this, the resist components must be soluble in and inert toward the selected coating solvent or medium, the formulation must form glassy films without component precipitation, separation, or dewetting, and must be stable during postapplication heating steps. A variety of different coating techniques have been applied, including spray-coating, curtain-coating, spin-coating or whirling, dip-coating, dry-film lamination, and most recently, electrodeposition onto a conducting substrate from an aqueous emulsion of resist components.
- The coated film must display adequate *adhesion* to the substrate after coating, and through the develop and image transfer steps. Adherence is influenced by resist composition, substrate surface composition, preparation and cleanliness, coating conditions, develop and etch process details, and, with negative cross-linking resists, by the exposure dose. Adhesion loss in mild cases is manifested by the lifting of a resist pattern at its perimeter (often visible under microscopic examination as a contrasting band) and in extreme cases by complete detachment of the resist pattern.
- The resist must have suitable *radiation sensitivity*. Today's exposure tools are so costly that tool throughput is a key measure of performance. The overall time to expose a resist film is the sum of the times to load and position the substrate in the exposure tool, to align the substrate and the mask, to irradiate the film, and to unload the completed part. In the optimum case, the resist exhibits sufficient radiation sensitivity so that the fraction of the overall cycle apportioned to irradiate the film does not limit the number of substrates exposed in a given period of time.
- The resist must provide *high fidelity reproduction* of the mask image on the substrate. This attribute is generally quantified as the resist's resolution, ie, the smallest feature that can be consistently printed, and its contrast, which is a fundamental measure of how the resist response changes with increasing radiation dose. In high resolution lithography, diffraction and imperfections in the optical system cause stray radiation to be scattered into regions of the resist pattern that nominally are unexposed. A resist with high contrast can effectively reject the stray radiation and yield a more accurate replica of the original mask. Resist contrast and resolution are influenced by its composition, by process conditions, and exposure tool characteristics.
- The patterned resist must provide an effective *protective barrier* during image-transfer. The image-transfer step frequently includes harsh chemical or physical treatments that erode or otherwise degrade the resist pattern. A resist's capacity to withstand the more vigorous image transfer processes (eg, plasma etching) can vary widely with its composition.
- After image transfer, the patterned resist must be readily and completely *removable* without substrate damage. The pattern often can be stripped from the substrate with a mild organic solvent. Proprietary stripper formulations or plasma oxidation treatments are utilized when the imaging chemistry or image transfer process has insolubilized the pattern.

3. Historical Development of Resist Materials

Most modern lithographic resists are evolved from materials first developed for the printing industry . Increasingly, specialized resists and processing techniques have been introduced as applications of lithographic technology have grown in scope and sophistication.

3.1. Early Photoresists. The first compositions widely used as photoresists combine a photosensitive dichromate salt (usually ammonium dichromate) with a water-soluble polymer of biologic origin, such as gelatin, egg albumin (proteins), or gum arabic (a starch). Later, synthetic polymers such as poly(vinyl alcohol) also were used . Irradiation with ultraviolet (uv) light (λ in the range of 360–380 nm) leads to photoinitiated oxidation of the polymer and reduction of dichromate to Cr(III). The photoinduced chemistry renders exposed areas insoluble in aqueous developing solutions .

Dichromated resists exhibit numerous processing shortcomings, and in the 1950s resist systems with substantially improved processing characteristics were developed. The first commercially available member of this class, KPR, was introduced in 1953 by Eastman Kodak. Originally targeted for printing applications, KPR was used in the fabrication of circuit boards and semiconductor devices later in the decade. This material is a cross-linking system based on the photodimerization of poly(vinyl cinnamate) chains. Pendant carbon–carbon double bonds on adjacent polymer strands undergo photocyclization to form a cross-linked, insoluble network in exposed areas.

Negative-acting resist compositions that combine an unsaturated hydrocarbon polymer derived from polyisoprene with an organic aromatic bis(azide) were introduced in the 1960s. These resists exhibited photosensitivity and adhesion significantly improved over available poly(vinyl cinnamate) systems. Numerous commercial formulations based on this chemistry have been marketed. The polymers in these resists are prepared by treating natural rubber derived from latex, or synthetic poly(isoprene), with a metal or acidic catalyst to induce partial ring formation along the chain. The resulting "cyclized rubber" product displays improved adhesion and flow characteristics with a softening temperature of $\sim 65^{\circ}C$, properties suitable for thin-film coating applications .

During exposure of the formulated resist, azide groups in the sensitizer undergo sequential loss of molecular nitrogen. Each fragmentation produces a highly reactive nitrene with two unpaired electrons. Cross-linking results when nitrene intermediates add to residual carbon–carbon double bonds or insert into carbon–hydrogen bonds, converting the matrix into an insoluble network.

First introduced for printing applications, bis(azide)–rubber resists were soon adopted by the developing microelectronics industry and used extensively for device fabrication through the 1970s. However, as the semiconductor industry refined manufacturing processes to further miniaturize integrated circuits, the limitations of this chemistry became apparent.

First, molecular oxygen dissolved in the film degrades the imaging chemistry. The nitrene intermediate reacts readily with oxygen to form azoxy and

nitroso products, in competition with addition and insertion and reducing the extent of polymer–polymer cross-linking. This leads to excessive film thinning (due to suppression of cross-linking near the air–polymer interface) and increased dose requirements. The traditional contact exposure technique was displaced by proximity- and projection-exposure methods (Fig.) in the 1970s in order to reduce device and mask damage by avoiding direct mechanical contact, and the change magnified the impact of this oxygen effect since the mask no longer acts as a physical barrier to prevent diffusion of atmospheric oxygen into the resist film during exposure.

A second limitation stems from the insolubilization mechanism operant in these resists. Photoinitiated cross-linking converts the polymer film from a glassy matrix of individual polymer strands into a cross-linked three-dimensional (3D) network that is effectively a single molecule bound to the substrate surface. Cross-linked and unexposed regions of the film are structurally similar and interact comparably with the developer solvent. The same intermolecular forces that are the basis for dissolution of the unexposed film can lead to considerable permeation of the developer into the exposed and cross-linked portions. The resulting swelling distorts the resist images, in unfavorable cases so severely that adjacent resist features contact and adhere. Both solvent-induced swelling and oxygen inhibition are characteristic of all cross-linking negative resists based on free-radical chemistry.

In 1968, E. I. du Pont de Nemours & Co. introduced an innovative resist system based on photoinitiated free-radical photopolymerization (PIP) and supplied in the form of a multilayered "dry film" structure . The attractive aspect of PIP is that each initiator species produced by photolysis launches a cascade of chemical events, effectively forming multiple chemical bonds for each photon absorbed. The gain that results constitutes a form of "chemical amplification" analogous to that observed in silver halide photography, and illustrates a path for achieving very high photosensitivities. In this material, marketed under the trade name Riston, the polymerizable imaging layer includes a mutlifunctional monomer and a photosensitizer to generate a flux of initiating free radicals. This layer is sandwiched between a polyolefin carrier sheet and a transparent polyester cover sheet (Fig.). The resist is applied by removing the carrier sheet and laminating the polymerizable layer to the substrate using heat and pressure. The cover sheet is left in place, both to protect against contamination and to act as a diffusion barrier against atmospheric oxygen during exposure. Prior to developing the image the cover sheet is peeled away. Today there are a number of commercial resist products marketed in dry-film format and are in wide use for the fabrication of printed wiring boards .

As PWB technology is refined to provide greater integration using finer conductor lines, there is renewed interest in liquid resists. The absence of a cover sheet and the ability to apply thinner films both contribute to improved resolution and to an intrinsically lower consumables cost .

3.2. Resist Materials for Imaging with Ionizing Radiation. Although most lithographic processing uses light in the visible to uv wavelength region (known as photolithography), a number of specialized, low volume applications employ high energy radiation and have unique resist requirements as a result. These include very high resolution lithography techniques using beams of elec-

trons or X-rays to induce chemical changes in the resist film. Electron beam or e-beam lithography is used extensively for the fabrication of high resolution photomask patterns, and for direct writing or circuit patterns for low volume, custom microelectronic applications . Though the applicability of proximity-mode X-ray lithography in large-scale device fabrication has been extensively researched it is unlikely to be used in that capacity since photolithography has been extended to image resolutions well beyond those first anticipated. At present, the principal commercial application of X-ray lithography is the LIGA (a German acronym for lithography–electroplating–molding) process for forming micromechanical parts . A soft X-ray projection exposure technology with resolution superior to proximity X-ray techniques is now under development for future use and will be described later in this article.

In e-beam lithography, a finely focused beam of high energy electrons is scanned in a pattern across a resist-coated substrate. Collisions of impinging (primary) electrons and secondary electrons with atoms of the resist film produced ionic and radical species that undergo further reaction, modifying properties of the surrounding matrix. In X-ray lithography, initial absorption of a photon produces an energetic photoelectron whose collisions with atoms of the resist lead to the same intermediates produced by e-beam radiation. For this reason, there tends to be a correlation between the sensitivity of a resist material for electron beam and X-ray lithography. However, the chemistry differs substantially from that caused by nonionizing (ie, long wavelength uv to visible) radiation, so that there is no assurance that a resist designed for photolithography will be found suitable for these methods.

Many examples of positive- and negative-tone X-ray and e-beam resists have been described . A number of these are single-component systems consisting of a polymer with intrinsic radiation sensitivity. If radiation-induced cross-linking is the predominant reaction, then the resist is negative acting. Conversely, if chain scission and/or depolymerization are the principal reactions, then the polymer functions as a positive-tone resist. One representative example is a positive-tone resist developed by Bell Laboratories in the early 1970s that has been widely applied to commercial photomask manufacture by electron-beam lithography . This resist is the polymer poly(butene-1-sulfone) (PBS), an alternating copolymer of butene and sulfur dioxide (Fig.). Electron-beam irradiation of PBS is believed to produce a cation radical center initially that destabilizes the chain. Scission at that site creates radical- and cation-terminated polymer strands that may undergo further fragmentation before deactivation.

4. Modern Resists for Microlithography

Figure shows one representation of Moore's law , which traces the evolution of semiconductor lithographic technology, as characterized by the minimum feature size versus the year of commercial introduction of the corresponding device generation. Also shown are the leading-edge exposure technologies that were introduced to support this drive to finer device dimensions. As we shall see, the

evolution of modern resists is the result of new materials requirements that arise as new exposure technologies are introduced.

Today the market for photoresists used in the manufacture of integrated circuits is estimated to be > $850 million annually . Both the mature diazonaphthoquinone–novolac resist products and more advanced commercial resist systems designed for deep-ultraviolet (duv) applications are used in significant volumes. Forecasts indicate that use of duv resists will continue to grow.

4.1. Positive-Tone Photoresists Based on Dissolution Inhibition by Diazonaphthoquinones. The intrinsic limitations of bis(azide)–cyclized rubber resist systems led the semiconductor industry to shift to a class of imaging materials based on diazonaphthoquinone (DNQ) photosensitizers. Both the chemistry and the imaging mechanism of these resists (Fig.) differ in fundamental ways from those described thus far . The DNQ acts as a dissolution inhibitor for the matrix resin, a low molecular weight condensation product of formaldehyde and cresol isomers known as novolac . The phenolic structure renders the novolac polymer weakly acidic, and readily soluble in aqueous alkaline solutions. In admixture with an appropriate DNQ the polymer's dissolution rate is sharply decreased. Photolysis causes the DNQ to undergo a multistep reaction sequence, ultimately forming a base-soluble carboxylic acid that does not inhibit film dissolution. Immersion of a patternwise-exposed film of the resist in an aqueous solution of hydroxide ion leads to rapid dissolution of the exposed areas and only very slow dissolution of unexposed regions. In contrast, with cross-linking resists, the film solubility is controlled by *chemical* and *polarity* differences rather than molecular size.

The DNQ–novolac resists exhibit several important practical attributes. First, DNQ photochemistry is not inhibited by oxygen, so unlike free-radical based systems the resist can be exposed in noncontact modes with unimpaired imaging properties. Second, films of the resist develop in aqueous base by reactive dissolution process, with little or no swelling. This is because only the ionic, deprotonated phenolate form of the polymer is sufficiently polar to be solubilized by the aqueous developing solvent. Finally, the developing solvent is nonflammable and water based, an advantage from the viewpoints of workplace safety and materials handling and disposal.

The DNQ–novolac resist chemistry has proved to have remarkable flexibility and extendibility. First introduced for printing applications, DNQ–novolac resists have been available since the early 1960s in formulations intended for electronics applications. Though more modern resist chemistries are used to manufacture today's most advanced semiconductor products, many microelectronics manufacturing processes continue to employ DNQ–novolac resists. One large volume use is in the fabrication of thin-film transistor circuitry for flat panel video displays.

Careful research and materials engineering have led to extensive refinement of this family of materials. Structural variation of the ballast or backbone group of the DNQ sensitizer has been explored in great depth. By correlating structure and lithographic properties, researchers have identified numerous factors that can influence resist performance. These include the number of diazonaphthoquinone sulfonate groups per sensitizer molecule , the spatial proximity of those groups , the backbone's size and the degree of esterification of

polyfunctional DNQs , backbone hydrophobicity , and DNQs capacity for hydrogen bonding with the phenolic matrix resin .

Novolac resins used in DNQ-based resists are condensation products of phenolic monomer (typically cresols or other alkylated phenols) and formaldehyde, formed under acid catalysis. The characteristics of the polymerization chemistry of novolacs lead to product with a very low average molecular weight, with a multimodal molecular weight distribution. Lithographic properties of DNQ–novolac resists are strongly influenced by polymer molecular weight characteristics and by the mixture of phenolic monomers in the polymerization feed. For example, in one study, dissolution rates of both exposed (R_e) and unexposed (R_u) resist films were shown to decrease with increasing molecular weight, though the ratio of these rates, R_e/R_u, a measure of contrast, was found to be independent of molecular weight . This same study also found that molecular weight distribution influences resist contrast, which improves with increasing polydispersity until a maximum contrast is attained. Numerous studies have probed how novolac microstructure influences resist lithographic properties. In one example, a series of resists were formulated from novolacs prepared with varying feed ratios of *p*-/*m*-cresol. These researchers found that the dissolution rate decreased, and the resist contrast increased, as the *p*-/*m*-cresol feed ratio increased . Condensation can only occur at the ortho position of *p*-cresol, but can occur at both the ortho- and para positions of *m*-cresol. It is believed that increased steric factors and chain rigidity that accompany increased *p*-cresol content modify the polymer solubility.

4.2. Deep-Ultraviolet Chemically Amplified Resists Based on Acid Catalysis. In any optical imaging system, the size of the smallest element that can be accurately resolved is related to the wavelength of exposing light: The smaller the wavelength, the finer the feature that can be resolved . In the microlithographic arena, improved resolution is achieved by incrementally shifting the exposure wavelength to smaller values as refinements in optics, tooling, and process technology permit. Figure details this trend. During the 1990s, the microelectronics industry made the transition from exposure tools designed to use monochromatic light at $\lambda = 436$ and 365 nm (two strong emission lines in the spectrum of mercury arc lamps) to more advanced exposure tools that use light at 248 nm (the output wavelength of a krypton fluoride excimer laser), in the duv region. This wavelength shift has profound implications from the viewpoint of resist design. The DNQ–novolac resists, once the industry standard, are impractical for duv photolithography for two reasons.

The first can best be illustrated by consideration of resist optical properties. Figure **a** shows the optical absorption spectrum of a typical DNQ–novolac photoresist film before and after exposure with 365-nm light. The absorption band at long wavelengths (300–450 nm) is that of the DNQ sensitizer. As the DNQ is photolyzed, this characteristic absorption decreases. The increased transparency facilitates efficient photolytic conversion of the sensitizer throughout the depth of the film. If such a film is exposed at 248 nm, however, the strong nonbleaching absorbance at the wavelength (due in part to the novolac matrix polymer, and in part, to the DNQ and its photoproduct) sharply attenuates the beam as it passes through the film. The result is highly nonuniform photolysis of photosensitizer in

the resist film, with insufficient conversion near the substrate interface. Figure **b** and **c** illustrates the damaging effect on resist imaging properties.

Second, the overall brightness of light sources available for duv exposure is much less than that of mercury arc lamps used for 365-nm wavelength. Though KrF excimer lasers are generally regarded as powerful sources of uv light, the spectral output line is relatively broad. Limitations of available lens materials make correction for chromatic aberration difficult, so the source output beam must span only a very narrow wavelength range. Introduction of optical line narrowing elements into the beam leads to a large overall attenuation. Roughly speaking, a photoresist designed to be used with duv exposure tooling now at hand must be at least 10-fold more efficient in its utilization of absorbed photons than a DNQ–novolac resist. Since the quantum yield for DNQ–novolac systems is on the order of $\sim$0.3, a 10 $\times$ improvement in efficiency is a considerable challenge.

One potential approach extends the idea of chemical amplification introduced in our preceding discussion of dry-film resists. In 1982, Ito and coworkers recognized that if a photosensitizer producing an acidic product is photolyzed in a polymer matrix containing acid-labile groups, the acid will serve as a spatially localized catalyst for the formation or cleavage of chemical bonds.

An early practical example of this concept is shown in Fig. . The acid-generating sensitizer is an onium salt, a class of compounds that efficiently generate a Brønsted acid upon photolysis. The polymer is poly(*tert*-butoxyoxycarbonylstyrene) (PTBOCST). Photolysis forms a small quantity of acid in those areas exposed to radiation. During a later heating step the acid catalyzes thermolysis of pendent *tert*-butoxyoxycarbonyl (TBOC) groups, converting the nonpolar PTBOCST into the polar poly(hydroxystyrene) (PHOST) and gaseous products, while regenerating the initial acid. The converted latent image can be developed in either positive tone by selecting a polar solvent, or in negative tone by selecting a nonpolar solvent as the developer. The catalytic chain length for this system, the average number of TBOC groups fragmented by each acid molecule, has been measured to be in the range 800–1100 . Therefore only extremely low exposure doses (in the range of 1–5 mJ/cm^2) are needed to image this system, which is roughly two orders of magnitude more photosensitive than typical DNQ–novolac resists.

Since the original proof of concept, and a later demonstration of its practical use in semiconductor manufacturing , applications and extensions of this concept have proliferated. In the following sections, these systems are described in greater detail with emphasis on the resist formulation at a components level .

Photoacid Generators. Practical applications of photoacid generators (PAGs) have been actively pursued since onium salts were first reported to serve as photopolymerization catalysts in the 1970s . Onium salts are particularly useful as photoinitiators since they generate both Brønsted acids and free radicals and consequently can simultaneously initiate both cationic and radical cures. Owing to the high quantum efficiency for acid production, these ionic PAGs are well suited for chemically amplified photoresist applications. Onium salts are one of several classes of photoacid generators. A variety of other PAG compounds (both ionic and nonionic) have been developed as researchers have

sought to optimize the key functional properties that include the quantum yield of acid generation; photoacid characteristics such as acid strength (pK_a, volatility and mobility); wavelength response; solubility; thermal stability; toxicity and manufacturing costs. In the following sections, the properties of photogenerators of strong Brønsted acids and their use in microlithography are summarized.

Ionic Photoacid Generators. Ease of synthesis, high thermal stability, and good quantum yield have made sulfonium and iodonium salts the most widely used onium salts. Figure depicts some representative examples.

By altering the counterion in these salts (generally accomplished by a metathesis reaction) the properties of the photoacid can be readily modified, often without significant impact on the photochemical reactivity of the cation. In this way, the acid strength of the photogenerated acid can readily be varied from that of so-called "super acids" to the comparatively weak organic acids . Other modifications, such as the use of sterically bulky counterions (eg, substituting camphorsulfonate for methanesulfonate anion), have been studied in attempts to reduce acid volatilization and mobility .

The solubility properties of the PAG itself can play an important role in the overall resist performance as well . Solubility differences between the neutral onium salt and the acidic photoproducts can be quite high and will affect the resist contrast. In fact, onium salts can serve as dissolution inhibitors in novolac polymers, analogous to diazonaphthoquinones, even in the absence of any acid-sensitive chemical function .

Simple aryl onium salts absorb below a wavelength of 330 nm, making them well suited for applications requiring duv exposure. Spectral response can be shifted to longer wavelengths either by varying the substituents (Fig. **d**) or by sensitization. Aromatic hydrocarbons with low oxidation potentials have been used to shift the activity of the PAG to wavelengths >500 nm via electron-transfer sensitization . The absorption properties can also be shifted to shorter wavelengths by employing aliphatic substituents in the PAG (Fig. **c**). The chemical pathways leading to acid generation for both direct irradiation and photosensitization (both electron transfer and triplet mechanisms) are complex and at present not fully characterized. Radicals, cations, and radical cations all have been proposed as reactive intermediates, with the latter two species believed to be sources of the photogenerated acid (Fig.) . In the case of electron-transfer photosensitization, aromatic radical cations (generated from the photosensitizer) are believed to be a proton source as well .

Nonionic Photoacid Generators. Examples of such materials are listed in Fig. , and include a variety of structural types that may undergo several different photochemical rearrangements. As one example, irradiation of the 2,6-dinitrobenzyl ester shown in Fig. **a** results in an intramolecular rearrangement [the well-known *o*-nitrobenzyl rearrangement] ultimately producing toluenesulfonic acid . In this case, no radical flux is produced upon photolysis, minimizing the possibility of cross-linking side reactions that can lead in some cases to resist scumming or even negative-tone behavior in positive resist systems . In another type of photochemical reaction, electron transfer from a photoexcited phenolic moiety of the polymer matrix to a ground (electronic) state PAG molecule (analogous to the sensitization depicted in Fig.) leads to the formation

of methanesulfonic acid . Finally, 4-sulfonyl DNQ sulfonic acid generators (Figure **d**) have been used as PAGs in CA resists, most effectively at exposure wavelengths longer than 300 nm.

To achieve the best overall resist performance, the optimum PAG for a given resist system, whether ionic or nonionic, must balance the functional properties listed earlier in this section. The development of new photoacid generators, and the characterization of their functional properties, are considered key to the design of resists with increased levels of performance.

Acid-Catalyzed Chemistry. Acid-catalyzed reactions form the basis for essentially all chemically amplified resist systems for microlithography applications . These reactions can be generally classified as either cross-linking (photopolymerization) or deprotection reactions. The latter are used to unmask acidic functionality such as phenolic or pendent carboxylic acid groups, and thus lend themselves to positive tone resist applications. Acid-catalyzed polymer cross-linking and photopolymerization reactions, on the other hand, find application in negative tone resist systems. Representative examples of each type of chemistry are listed below.

Acid-Catalyzed Chemistry in Positive-Tone Photoresists. The ester, carbonate, and ketal acidolysis reactions that form the basis of most positive tone CA resists are thought to proceed under *specific acid catalysis* . In this mechanism, illustrated here for the hydrolysis of *tert*-butyl acetate (type $A_{Al}1$) , the first step involves a rapid equilibrium where the proton is transferred between the photogenerated acid and the acid-labile protecting group:

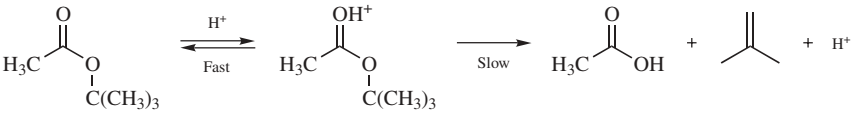

The rate of the reaction in such case is $R = k[PH^+]$, where P is the reactant (ie, a repeat unit bearing the acid-labile protecting group).

In resist systems the situation is more complex than that just outlined. The photogenerated acids can be so strongly acidic that they dissociate completely upon formation. In such case, the proton resides on other basic components of the resist film, which can include polymer functionality (ie, ester or ether comonomers), adventitious impurities such as water or residual casting solvents, as well as additives such as coating aids. The reactant PH^+ will be in equilibrium with all other protonated species in the resist film. The concentration of each protonated species is then determined by the basicity of its unprotonated conjugate. As deprotection proceeds, the concentrations of the basis resist components changes, shifting the equilibria and influencing the overall kinetics. Substitution of an acid of different strength, or introduction of a basic impurity or additive, perturbs the concentration of PH^+, and thereby, the imaging behavior of the resist.

Figure lists representative acid-labile protecting groups that have been incorporated in positive-tone CA resist systems. These groups can be pendent to the matrix polymer chain, can be attached to a monomeric or polymeric addi-

tive that acts as a dissolution inhibitor , or can even be appended to the PAG structure .

Acid-Catalyzed Chemistry in Negative-Tone Photoresists. Many negative-tone CA resist employ acid-catalyzed cross-linking to effect insolubilization of the exposed pattern. These systems function in a manner analogous to radical-based cross-linking resists, in some cases exhibiting the same limitations. One of the first CA resist systems described in the chemical literature is based on the acid-catalyzed cross-linking of epoxy groups (Fig. **a**) . Although such resists display excellent photospeed and are immune to inhibition by molecular oxygen, they suffer from the same solvent-induced image distortion during development that is seen with radical cross-linking resists. Careful attention to formulation and process conditions is required to achieve high resolution imaging. These difficulties, coupled with the practical problems associated with the use of organic solvents in a manufacturing setting, have limited the acceptance of such resists.

Several CA negative-tone photoresists based on PHOST polymers incorporate the cross-linking chemistries shown in Fig. **b** and **c**. The phenolic structure renders these systems developable using aqueous alkaline solutions. Dissolution properties of this type of cross-linking resist closely resembles the surface limited etching found in DNQ–novolac positive resists, so image distortion due to solvent swelling is not observed. Systems have been described where the active cross-linking group is covalently bound to the polymer , or is incorporated as a nonpolymeric additive . Cross-linking can occur at the phenolic hydroxyl site or on the ring via electrophilic aromatic substitution reaction, as shown in Fig. .

Although cross-linking systems have been most widely studied, negative-tone patterning can be achieved by exploiting the polarity change that accompanies deprotection. For example, the TBOCST resist (Fig.) produces negative-tone relief images when developed in a nonpolar organic solvent.

Processing Characteristics of CA Resists. While the increased radiation sensitivity afforded by CA resists offers enormous practical advantages, it brings the need for far more stringent control of the lithographic process. Any factor that influences the course of the catalytic reaction will have an effect that is amplified by a factor equal to the catalytic chain length.

Postexposure Bake (PEB) Temperature Control. The kinetics of acid-catalyzed deprotection vary significantly with structure. Each class of protecting group can be characterized by its activation energy E_a for acid-catalyzed deprotection, which quantifies how the rate of that reaction changes with temperature. This parameter has a large impact on CA resist processing characteristics. For example, acidolysis of the ester group in *tert*-butyl methacrylate (Figure **a**) has a relatively high E_a [measured to be 35 kcal/mol in experiments in resist films], and resists based on this chemistry require postexposure processing at temperatures of 120°C or higher. Experience has shown that for such CA resists, precise temperature control is required to achieve reproducible high resolution imaging. The temperature across the entire wafer (which in today's manufacturing processes can be up to 300 mm in diameter) typically must be uniform to better than 0.5°C during PEB.

The sensitivity of a CA resist's PEB process to small changes in temperature has been assessed by measuring the shift in the width of the final printed image with temperature . Correlations between the E_a of the deprotection reac-

tion and the magnitude of the image dimensional shift with temperature have been noted. The image shift in PTBOCST resist (E_a for deprotection ~28 kcal/mol) has been measured to be 40 nm/°C . In contrast, resists based on low E_a chemistry (eg, the acetal–ketal type system shown in Fig. **a**) undergo deprotection at or near room temperature and will exhibit little variation in final image line width with processing temperature . The image shift for measured for a CA resist based on acid-catalyzed acetal deprotection (E_a~15 kcal/mol) shows essentially no dimensional shift with temperature . Another potential advantage of these low E_a systems is a reduced dependence on the precise timing of processing since there is in effect no delay between the exposure and postbake steps. Deprotection at room temperature is not always desirable, however, as the outgassing of volatile deprotection products can contaminate internal surfaces of the exposure system, and the intrinsically higher reactivity can reduce the stability of the formulated resist solutions during storage (ie, its shelf life).

Processing Delay Time Effects. A critical, and at-first puzzling problem, was encountered during early manufacturing trials of CA resists. Sporadically, severely distorted resist profiles would be formed in positive-tone CA resists, displaying what seemed to be a cap on the upper surface of the resist image (Fig.). In severe cases, this cap or T-top would appear as a skin or crust over the entire wafer surface that prevented development of the pattern. The magnitude of the effect varied dramatically between laboratories and appeared to grow more severe as the time interval between exposure and postexposure bake was increased.

Ultimately, it was demonstrated that contamination of the resist surface by airborne basic impurities caused neutralization of the photogenerated acid near the resist–air interface, suppressing the acid-catalyzed chemistry, and thereby producing the observed effects. *N*-Methyl-pyrrolidone (NMP), a common solvent used in semiconductor manufacturing as a stripping and coating solvent, was the first basic contaminant to be identified in laboratory air . Even though an amide like NMP is generally considered to be a weak base [the pK_a of protonated NMP is ca. −1.0] when compared to the basicity of the polymer matrix (the pK_a of most protonated esters, ethers, and phenols is in the range of −6 to −7), NMP is sufficiently basic to compete effectively for the proton catalyst, slowing the rate of the deprotection reaction (and the overall extent of conversion) in the contaminated region of the resist film. Other sources of airborne clean room contaminants now have been identified . These include paints, adhesives and sealants, materials that, like NMP, cannot be readily eliminated from the semiconductor manufacturing process.

The impact on negative-CA resists of airborne base contamination differs qualitatively from their positive tone counterparts. Suppression of acid-catalyzed chemistry at the surface of a negative resist results in some film erosion at the top of the exposed fields and in some cases an apparent loss of photosensitivity, but in general the relief images formed exhibit the expected cross-sectional profile. This is in sharp contrast with the typical behavior seen with positive-tone CA resists, where suppression of acid-catalyzed chemistry at the surface causes an insoluble surface skin.

Three approaches have been identified that reduce susceptibility of CA resists to airborne contamination. In the first, process engineering changes

such as the addition of special activated carbon filters to the environmental chambers surrounding the exposure tools , overcoating the resist with a soluble protective film to isolate the resist from the environment , or modifications of the process flow to minimize the time interval between exposure and post-exposure bake have been shown to improve CA resist processibility.

A second approach modifies the CA resist chemistry. For example, researchers have introduced basic additives into the resist formulation to minimize the impact of surface contamination of the resist film . A resist that already contains added base (and consequently requires a larger imaging dose) should be less affected by the absorption of small amounts of basic contaminants. Systems of this type have been claimed to have improved resolution as well. The rationalization here is that the acid that diffuses into the unexposed regions of the resist film is neutralized and does not contribute to image degradation .

In the third approach, improved resist process stability in the presence of airborne bases is realized by consideration of how this stability is influenced by properties of the resist polymer. Using radiotracer methods to tag the basic contaminant, the kinetics and extent of contaminant uptake can be quantified . In one study, a wide range of polymer structures were cast as thin films on silicon wafers, and then stored in air containing a known, very low concentration of ^{14}C-labeled NMP . The rate of NMP uptake was found to vary by almost a factor of 50 depending on the polymer structure. The contaminant uptake of each polymer could be related to its physical properties, specifically its solubility parameter and its glass transition temperature (T_g). The correlation between NMP uptake and polymer T_g (Fig.) was attributed to a reduction in free volume (a consequence of the nonequilibrium nature of the spin-coating process) due to polymer film annealing during postapply baking, thereby reducing diffusant mobility.

One practical conclusion that can be drawn from this result is that susceptibility to airborne chemical contaminants can be minimized if a CA-resist film is baked after coating at a temperature at or above its T_g. However, at that time few existing resist systems had sufficient thermal stability to allow such treatment . By deliberately selecting polymer, protecting groups and PAGs with thermal stability in mind, however, CA resists can be designed that can be heated at or above T_g . Such resists display sharply improved environmental stability compared to analogous systems processed $< T_g$.

Polymers for 248-nm Chemically Amplified Resists. Earlier it was noted that novolac-based resists are too strongly absorbing at 248 nm to be used for duv exposure. Many derivatives of PHOST are sufficiently transparent at 248 nm to provide a phenolic platform for resist design. Figure compares the optical absorption characteristics of PHOST and novolac polymers. Resists used in duv lithography are typically copolymers of hydroxystyrene and an acid-labile comonomer, often a protected hydroxystyrene, as depicted in Fig. . These polymers are almost always produced by free-radical solution polymerization of a derivative of 4-hydroxystyrene (HOST), and thus, are usually medium molecular weight polymers with a relatively narrow polydispersity (between 1.5 and 2.5) . As detailed earlier, the unique properties of novolacs stem in part from the unusual condensation polymerization mechanism which produces substantial quantities of oligomeric products and high molecular weight branched

polymer. Analogous fractions are not produced in the polymerization of protected hydroxystyrenes. The functional properties of phenolic resins based on HOST bear little resemblance to those of novolacs, even though the polymers are structurally similar (in fact, isomeric).

The use of CA resists based on phenolic polymers for 248-nm duv applications is now firmly established and widespread. Today, the most advanced microelectronic devices are fabicated using resists designed for imaging with light of $\lambda = 193$ nm. As before the change provides an improvement in resolution in proportion to the wave length reduction.

Polymers for 193-nm Resists. Phenolic polymers in many respects are ideal for microlithographic resists as they provide predictable, well-controlled dissolution behavior, excellent adhesion properties, and acceptable plasma etch resistance. But the strong absorption of phenolic polymers at 193 nm (illustrated in Fig.) precludes their use at that wave length, and a decade-long effort to develop high performance resist materials to support 193-nm exposure technology can be characterized as the pursuit of new transparent polymer systems that combine these three functional attributes as effectively as do their phenolic counterparts.

193 nm Resist Design Strategies. For a typical target thickness of ~400 nm, the ideal optical density of the formulated resist should be on the order of 0.2–0.3, representing a balance between conflicting requirements for high transparency to provide uniform illumination through the depth of the film, and efficient light absorption to attain high photospeed. This transparency requirement precludes the use of unsaturated functionality such as aromatics and vinylics, but aliphatic, cycloaliphatic, carboxylic ester and acid, ether, nitrile, and sulfone groups exhibit acceptable optical properties. Using such nonaromatic building blocks, resist chemists have worked to achieve both good plasma etch resistance and good lithographic performance. Experience has shown that this calls for a balancing of the at-times-conflicting properties of the building blocks through copolymerization and blending.

Analyses of the relation between polymer structure and plasma etch resistance have led to a set of guidelines applicable to resist design . Polymer materials with "cyclic carbon", ie, those having a significant mass of carbon in the repeat unit incorporated as ring structures with high C–C connectivity, exhibit improved etch resistance . In 193-nm resist materials, the restriction against incorporating aromatic structures reduces this to a simple rule: Maximize the alicyclic groups (aliphatic rings) in the polymer to maximize etch resistance. The alicylic structure can be integrated into the polymer chain, or can be incorporated as inert or acid-labile pendant groups .

Perhaps the most significant challenge in the design of 193-nm resists is the control of dissolution properties in 0.26 *N* aqueous tetramethylammonium hydroxide, the industry-standard developer solution. Transparent, base-labile functional groups such as carboxylic acids and anhydrides and lactones have emerged as functional substitutes for phenols. The dissolution behavior of carboxylic acids differs markedly from that of phenols, presumably due to the much stronger acidity of the former, which affects the extent of ionization and therefore the polarity of the ionized chains when contacted by developer. While the inclusion of a large proportion of alicyclic groups improves polymer etch

resistance, the added hydrophobic character further complicates its dissolution behavior. By reaching the proper hydrophilic–hydrophobic balance it is possible to achieve a large difference in solubility between exposed (deprotected) and unexposed resist, at useful dissolution rates and without swelling. To further tune solubility properties, low molecular weight aliphatic dissolution inhibitors (often cholate esters) frequently are added to 193-nm resist formulations . The inclusion of such compounds allows more flexible control of dissolution properties and acts to plasticize the film, a benefit at times since several of the polymer systems under study for 193-nm resists have very high T_g (200°C or more). More recently, pendent functional groups based on hexafluoroisopropyl alcohol (HFIPA) have been included in the polymer structure to control dissolution properties. The HFIPA group has an acidity close to that of phenol , and its inclusion in a polymer moderates the impact of the carboxylic acid groups on dissolution. Unlike phenol, the HFIPA group is transparent at 193 nm.

Research efforts in 193-nm resists in large part have focused on three polymer families: poly(acrylates), poly(cycloolefins), and cyclic olefin–maleic anhydride (COMA) copolymers. The main characteristics of each of these are detailed below.

Acrylic Polymers for 193-nm Resists. Acrylate and methacrylate polymers as a class are quite transparent in the 193-nm spectral range (Fig.). Positive-tone CA resists based on acrylic polymers, though first designed for printed circuit fabrication where minimum dimensions are 50 μm or more, have been demonstrated to produce high resolution images using 193-nm exposure tooling .

The methacrylate terpolymer shown in Fig. **a** typifies this class of material. In the terpolymer, each monomer type imparts specific characteristics to the polymer, providing a mechanism for precise balancing of functional properties. The polymer contains a protecting group (acid labile), a more polar group that improves adhesion and solubility of the PAG in the film, and a smaller amount of a carboxylic acid to modify film polarity and dissolution. Such polymers are prepared by simple free-radical solution polymerizations that are readily scalable to manufacturing levels. The copolymerization properties of methacrylate monomers, where the ester groups exert little influence on reactivity toward polymerization, make it straightforward to optimize resist properties by synthesizing ter- or tetrapolymers.

The etch resistance of common acrylic polymers is poor but can be improved without reducing 193-nm optical transparency by the attachment of alicyclic pendant groups to the backbone. For example, a 1:1 copolymer of *tert*-butyl methacrylate and adamantyl methacrylate exhibits a nearly twofold reduction in plasma etch rate compared to the *tert*-butyl methacrylate homopolymer. Figure **b** provides examples of alicyclic ester groups that have been assessed .

Acrylate polymers slowly undergo chain scission upon irradiation with uv light and electron beams. While this property has been used to advantage (acrylic polymers such as poly(methylmethacrylate) have seen use as high resolution but low sensitivity electron beam and duv resists), in this instance it is undesirable as it compromises plasma etch resistance, and complicates the metrology of acrylate resist patterns when using scanning electron microscopy .

Cyclic Olefin Polymers for 193-nm Resists. These resists have received significant attention, as the base polymers are extremely robust in plasma etch processes . Figure depicts illustrative examples of this class of polymer that have been examined for 193-nm lithographic applications . The polymers typically are prepared by means of a metal-catalyzed addition or ring-opening metathesis polymerization process using substituted norbornene monomers. Polymers prepared by the metal-catalyzed addition have relatively low molecular weight (3–10 K M_w), polydispersities of $\sim$1.5 and very high glass transition temperatures ($> 250^\circ$C). In the ring-opening process, product molecular weight can be controlled over a wide range by the addition of α-olefins to the polymerization mix. Cyclic olefin-based resists have been notable for their atypical development properties in aqueous base (a tendency toward significant swelling), but nonetheless have been used to formulate resists capable of high resolution imaging properties.

COMA Copolymers for 193-nm Resists. Introduction of an anhydride linkage into the cyclic olefin polymer structure leads to a significant and useful improvement in dissolution properties (Fig.): COMA copolymers require a much lower proportion of carboxylic acid to achieve aqueous dissolution, and that dissolution proceeds without the substantial swelling that is characteristic of cyclic olefin polymers . Hydrolytic ring opening of the anhydride during development, producing a hydroxyl group and a carboxylate anion in the alkaline developer medium, occurs synchronously with development. Presumably the additional ionization of the backbone increases its rate of dissolution such that swelling is minimized.

The COMA polymers, synthesized by conventional radical polymerization, have a 1:1 alternating structure, a consequence of the preference for each radical to react exclusively with the other monomer. As a rule, the products are high T_g materials; for example poly(norbornene-*co*-maleic anhydride) has a $T_g > 300^\circ$C. The polymerization allows the incorporation of small amounts of other vinyl monomers (eg, acrylic acid) without disruption of the alternating structure . Substituted norbornenes can be included in the polymerization mixture to incorporate acid-labile functionality, to modify polymer polarity and to improve film adhesion . Cholate dissolution inhibitors can be added in the formulated resist to further modify functional properties .

Vinyl ether monomers also have been combined with maleic anhydride to prepare alternating copolymers. Conceptually similar to COMA systems, these polymers have lower T_g and possibly improved imaging properties .

5. The Next Stage of Lithography : Extension to the Nanoscale

Industry planning calls for the pace of miniaturization in semiconductor technology to be maintained well into the future. This is depicted in Fig. as the dashed line segment that marks the anticipated timing for achieving finer critical dimensions. The most recent revision of the International Technical Roadmap for Semiconductors (ITRS) , which outlines target device and materials requirements for future generations of semiconductor devices, calls for device dimensions to shrink to 20-nm minimum size by the year 2017. For the ITRS 20-nm

technology node (the number specifies the dimension of an equal line-space pattern, the most stringent metric for lithographic spatial resolution), requirements are that the resist will be used at a film thickness between 40 and 70 nm, will exhibit a line-edge roughness (LER) of no > 0.7 nm/edge (3σ) and will support overall control of critical dimensions to 0.7 nm (3σ). These tolerances are smaller than the dimensions of the polymer molecules that constitute today's resists, and given a typical carbon–carbon bond length of 0.13–0.15 nm , it is clear that this specification is a call for near-atomic-scale control. Clearly, such milestones can only be reached by further refinement of lithographic tooling and resist materials.

Before describing the exposure technologies now under development for future use, and the implications each technology has for resist design, we will outline the common limiting resist factors that are being encountered as research in the sub-100-nm dimensional regime expands.

5.1. Resist Limits of Extendibility. Poly(methylmethacrylate) (PMMA) is capable of imaging line-space arrays (formed by electron beam lithography) at the 15–20-nm scale (30–40-nm pitch) without excessive LER , the current resolution record for a polymer-based resist material. The PMMA functions on the basis of electron-beam induced chain scission, and the molecular weight reduction that results increases the rate of dissolution of exposed areas in organic solvent developer mixtures . Its resolution limit has been attributed to restrictions imposed by molecular size, intermolecular forces and dynamics present during development, and nanoscale swelling . While the PMMA results provide encouragement that 20-nm scale lithography is achievable in principle, the radiation sensitivity of PMMA is inadequate by orders of magnitude for its use in semiconductor manufacture.

The resist sensitivities specified by the industry roadmap imply that future lithographic technologies will require CA resists that provide lithographic performance suitable to sustain their extension to dimensions < 20 nm. However, while CA resists are subject to the same factors that limit the spatial resolution of PMMA, their imaging mechanism adds chemical and physical effects that can further limit extendibility. The complete set of limiting factors, highlighted in Fig. , can be classified into several categories. First, *image blur effects* can limit extendibility. The presence of a concentration gradient of photogenerated acid at the vicinity of the final target line edge has long been recognized as a potential source of image blur that will impede efforts to improve CA resist resolution. Photogenerated acid created in the nominally unexposed regions of the resist pattern, the result of diffraction or scattering of the imaging radiation and found at low concentrations, is a second contributor to image blur. Second, *statistical effects* can restrict resist extendibility. The catalytic role of the photogenerated acid imparts increased sensitivity, but reduces the number of exposure events (either electromagnetic radiation or energetic particles) in inverse proportion to the amplification factor. For nanoscale features this can reduce the number of exposure events to a level, where statistical dose fluctuations cause a loss in imaging precision . This effect will be accentuated when high energy radiation sources are used. In the same vein, the number of acid molecules required to image a nanoscale structure can become so small that statistical fluctuations in their spatial distribution and in the turnover of indi-

vidual catalyst molecules can become evident. Statistical dissolution effects at the line edge, while not necessarily tied to the CA resist imaging mechanism, can add further to statistical variation. These statistical effects are manifested in the final image as fluctuations in the shape of the final relief image. Finally, *interfacial effects* acting on nanoscale resist relief images during processing can cause their mechanical fracture.

Image Blur in CA Resists. The mobility of the acid catalyst in the film influences CA resist performance, and various approaches to estimate acid mobility in CA resist films have been described . At the molecular level, the proton must move from site to site to effect acid catalyzed reactions in the resist film. If the mobility is too great, however, the initial spatial profile of photogenerated acid will be blurred and the final developed resist image will appear distorted. The problem becomes more acute at finer resolution. In those situations where diffusion of the positively charged proton causes a net displacement of positive charge, as is the case for diffusion in a concentration gradient, it must be accompanied by diffusion of the anion so as to maintain overall charge neutrality. In such cases, the proton movement is coupled to that of the anion, and those properties of the anion that affect its mobility, eg, its volumetric size, will influence the overall acid transport. The use of onium salts bearing sterically bulky counterions [eg, where camphorsulfonate anion (Fig. **e**) is used rather than methanesulfonate] has been examined as a means for reducing acid mobility .

While excessive acid diffusion leads to image blur, even in cases where diffusion has been suppressed to an insignificant level (eg, by means of an immobile anion), significant image spreading still will occur during PEB . When imaging at dimensions near the resolution limit of a projection exposure tool, diffraction leads to partial illumination, and therefore generation of some amount of acid, in areas of the resist that nominally are unexposed. Because of this, the deprotection reaction proceeds rapidly at the center of the exposed image but also at a significant though slower rate in the nominally unexposed regions. This causes the width of the deprotected region, which ultimately defines the shape of the developed image, to spread beyond the desired boundaries. Some early attempts to quantify acid diffusion convolved this chemical kinetic effect with true diffusion, leading to an overestimation of acid diffusion lengths, sometimes by an order of magnitude. This can be suppressed by purposely adding to the resist formulation a small amount of a basic substance such as an amine or an organic hydroxide . The amount of base is calculated to slightly exceed the amount of acid formed in the dark areas of the pattern, suppressing image spreading there with minimal impact on the chemistry in the exposed areas.

Overall image blur is controlled by the kinetics of both deprotection and acid diffusion. A dissection of the PEB kinetics for a representative model TBOCST resist system provides a quantitative assessment of the respective roles of chemical and transport kinetics . From such analysis the impact of image blur at nanoscale feature sizes can be modeled. Figure presents a prediction from such a model, which shows the spread of the final image from an hypothetical line 1 nm wide printed in TBOCST resist. In this case, the image spreads to $\sim$50 nm width due to photoacid diffusion, the effective resolution limit for this particular chemistry . This can be improved by reducing the ratio

of the average rate of catalyzed deprotection to that of transport, eg, by selecting a protecting group chemistry with a lower activation energy .

Line Edge Roughness. Random fluctuation in the width of a resist feature, termed line-edge roughness or LER, is anticipated to be a significant source of line width variations that could ultimately limit the extendibility of conventional lithographic resists to nanoscale fabrication. Analyses of imaged resists have revealed LER values that vary over a wide range . Figure depicts different forms of LER. Potential sources of LER include the molecular weight and molecular weight distribution of the resist polymer , the molecular structure of resist components , inhomogeneity in the distribution of resist components within the film , statistical effects influencing film dissolution , and intrinsic properties of the imaging chemistry .

The standard dimensional tolerance used in semiconductor fabrication is $\pm 10\%$ of the minimum feature size; eg, a minimum dimension of 50 nm will require dimensional control on the order of 5 nm. In resist patterns prepared under optimal imaging conditions, for a wide range of resist chemistries the minimum LER was found to be in the range 2–7 nm . This minimum roughness is on the order of the molecular size of polymers typically used in resist formulations, as estimated by the radius of gyration for polymers with molecular weights in the range of 5000–100,000. One factor that strongly influences the degree of LER is the sharpness of the aerial image; the more blurred the light image, the greater is the LER of the final resist image. This correlation is taken as evidence that nanoscale inhomogeneity in solubility properties is present at the intermediate dose range of the resist line edge and is replicated in the developed image.

Characterization of the origins of LER, and the design of strategies to minimize LER are today active areas of research. In recent work, experimental electron beam resist formulations comprised of nonpolymeric materials (eg, liquid crystals or fullerene derivatives) have displayed very high resolution (10-nm feature sizes) accompanied by very low LER ($\sim$1 nm or less).

Image Collapse. Though resist feature dimensions have undergone continuing reductions in linewidth, image thickness has not scaled proportionately. This is because significant erosion of the resist occurs during image transfer. While refinement of plasma etch processes has significantly reduced resist erosion, the improvements have not kept pace with the linewidth shrinkage. As a result the *aspect ratio* required of resist features, ie, the ratio of its height to its width, has increased with time as line widths have grown smaller. The extent to which the aspect ratio can increase ultimately is limited by mechanical failure of the images during processing, typically manifested as image collapse. Figure shows a typical example of this.

Studies of this problem have shown that the image collapse occurs following postdevelop rinsing of the nascent resist images . During the postrinse drying step, unequal surface tension forces from the rinse liquid trapped between features distort and then fracture the fragile structures. Isolated lines, which are not subjected to unsymmetrical forces, do not show image collapse.

The propensity for image collapse depends on the width and proximity of the features, its aspect ratio, the substrate surface and the mechanical properties of the imaged resist. Two characteristic failure modes have been identified: defor-

mation, where fracture occurs within the resist structure, and adhesion loss, where the resist feature separates from the substrate at their interface. Low surface tension rinse liquids [in the extreme, supercritical fluids], and the use of rigid and highly adhesive resists reduce the frequency of image collapse.

"Shot noise". The combination of high energy radiation, sensitive resists, and small feature dimensions reduces the number of exposure events required for imaging to such a degree that the expected random variation in that number from feature to feature can cause discernible and ultimately limiting variation in the feature size and shape. This has become known as the "shot-noise" effect. There have been numerous theoretical and experimental attempts to elucidate-shot-noise limits for proximity X-ray , e-beam , ion-beam and EUV lithographies, but the complexity of the lithographic process and the resist response make such analyses difficult . With CA resists, the postexposure bake chemistry and physics add to this complexity. A mathematical analysis of the statistics of acid generation, polymer deprotection, and development leads to the conclusion that these factors are at least as important as absorbed photon statistics .

5.2. Future Exposure Technologies. While a range of different revolutionary approaches to nanoscale lithographic resolution have been pursued (X-ray proximity , projection e-beam , and ion-beam lithographies), for large scale production the microelectronics industry currently is focusing its efforts on three candidates that are more evolutionary in character.

193-nm Liquid Immersion Lithography. The advantages afforded by introducing an index-matching fluid between objective and specimen were first recognized by Robert Hooke in his paper "Microscopium" presented to the Royal Society in 1678. The concept was elaborated in the 1800's by Brewster, Amici, Tolles and others. Today liquid immersion optical microscopy is a routine technique providing high resolving power. Since the same optical principles govern microscopy and projection lithography, a similar benefit can be realized in a lithographic setting by implementing liquid immersion in the optical projection exposure tooling. While this was first demonstrated in the 1970s , it was only in late 2003 that a formal effort to evaluate the practical implementation of liquid immersion lithography (LIL) was initiated.

The practical benefits and challenges of projection LIL have been analyzed , and detailed quantitative analyses of the optical implications of LIL have been carried out . Compared to a system with conventional air spacing, the liquid reduces the refraction of light in the region between the resist film and the final lens surface. This allows the optical lens system of an immersion exposure tool to be designed to increase depth of focus or to improve spatial resolution compared to its "dry" counterpart. The wavelength of the exposing radiation in the liquid is related to the wavelength in air by the inverse of the refractive index of the liquid. The refractive index of purified water at 193 nm is 1.44, so the exposing wavelength is effectively reduced to 134 nm, and the finest spatial resolution that can be achieved is improved in proportion to this wavelength reduction, much as a light source of shorter wavelength improves resolution in conventional projection lithography. Prior to the implementation of LIL, improved spatial resolution has been realized by increasing the energy of the exposing photons; this reduces the wavelength, but also increases the photon's frequency. In the LIL case, the energy and therefore the frequency of the expos-

ing photons is unchanged even though the wavelength is reduced compared to its value in air. Though optical absorption properties of materials often are described by referencing the wavelength (in air or vacuum) of the absorbed light, in fact they depend on photon *frequency* rather than *wavelength*.

The practical consequence of this for LIL is that the optical requirements for the resist materials are unchanged from conventional 193-nm dry lithography, so a major effort to develop new polymer platforms is not called for. However, the introduction of a fluid in contact with the resist film is a departure from conventional practice and significant effort has been directed at understanding the ramifications of this change. The added liquid–resist interface can foster materials transport into and out of the resist film, bringing the potential for contamination of the exposure tool optical surfaces with extracted resist components, and for interfering with the imaging chemistry and physics. Recent studies have established that onium salt photoacid generators and amine bases can be leached from 193-nm resist films by water, and that such films can absorb water at the level of a few parts per thousand over the time scale of an immersion exposure . In response, protective topcoat films to suppress materials exchange between resist and fluid are under development by several suppliers, as are resist components with decreased solubility.

157-nm Lithography. The next evolutionary step following 193-nm lithography would use the 157-nm emission of a molecular fluorine (F_2) excimer laser. Nearly all materials (most polymers and optical lens materials, and even atmospheric oxygen and water vapor) are strong absorbers at this wavelength, and this has slowed research efforts. First demonstrated in 1985 , serious feasibility studies of 157-nm lithography did not begin until the mid-1990s , when special mask substrates, optical materials, and purged exposure tools became available. At this time (early 2005), two technical issues uncovered in those feasibility studies, the intrinsic birefringence of CaF_2 used to fabricate optical lenses , and the absence of suitable materials for forming defect-reducing mask pellicles , have relegated this technology to backup status in favor of 193-nm LIL.

157-nm Resist Design Considerations. Like all resists, 157-nm photoresists must be designed to possess appropriate functional properties: adequate optical transparency, functional groups that confer aqueous base solubility, acid labile protecting groups to provide a solubility "switch" in exposed regions of the film, and acceptable plasma etch resistance. The overriding issue with polymers for 157-nm resists has been transparency. The exposure wavelength falls in the middle of the vacuum uv region of the electromagnetic spectrum, where electronic transitions of organic molecules consist of both excitations into Rydberg orbitals and valence shell transitions (ie, the $\Pi-\Pi^*$ transitions of aromatic molecules) found at longer wavelengths . Most organic materials have significant absorptions in this region of the spectrum . In particular, polymers used in 248- and 193-nm resists have absorbance values in the range of $6–8/\mu$, much too high for conventional resist applications even when thin films are used . As a class, polymers containing a high proportion of fluorine have been identified as providing suitable transparency . It is known that replacement of a hydrogen atom in a hydrocarbon framework with the highly electronegative fluorine atom has the general effect of raising the absorption frequency through perturbation of the σ-bonded framework . This effect can manifest itself over several centers. Of par-

ticular interest for resist materials, fluorinated alcohols and esters show decreased absorbance at 157 nm compared to their unfluorinated counterparts .

Earlier, we cited the use of fluorinated alcohols such as HFIPA in 193-nm resists, where their solubility in aqueous base is another result of the electron-withdrawing power of fluorine. Like phenols, fluorinated alcohols can be protected with acid labile groups, enabling their use in CA resist formulations. However, these partially fluorinated polymers tend to show poor plasma etch resistance. Though incorporation of alicyclic functionality can improve etch resistance significantly, 157-nm resists often show inferior etch performance compared to 193- and 248-nm resists . The usual PAGs and other additives, such as dissolution inhibitors , can be used to formulate 157-nm resist formulations provided they do not significantly degrade the resist transparency.

Figure shows several polymers that have been studied for 157-nm resist applications. While the base fluorocarbon polymers can show relatively low absorbance at 157 nm, modifications to incorporate etch resistant monomers and acid labile functionality often raise that absorbance substantially. In spite of this, CA resists with absorbance at 157 nm less than the target value of 1.0/μ of film thickness have been reported.

Multilevel 157-nm Resist Systems. It can be advantageous to separate the imaging and etch resistance functions of a resist into distinct polymer layers. Figure **a** shows schematically one approach that has been used in practice. Here, the image is confined to a thin photoresist overlayer. This layer is exposed and developed in the conventional manner, and the relief image that results is then transferred by an anisotropic dry etch process to a second thick polymer layer that then serves as the final etch resistant mask for substrate etching. By imaging only a thin resist layer, the absorbance requirements are relaxed, a significant advantage at 157 nm. Moreover, the etch resistance of the underlayer can be optimized without regard to optical transparency. Silicon-based imaging layers are particularly attractive here as they are resistant to oxygen reactive ion etch (RIE) conditions while conventional polymers are rapidly eroded. Silsesquioxanes are high silicon content materials that have been applied in a number of bilayer resists . Fluorocarbinol variants with minimal hydrocarbon content have acceptable transparency at 157 nm (Fig. **b**). These can be used to build positive tone resists by incorporating an acid-labile function, such as the *tert*-butoxy carbonate protecting group. Negative tone resists can be formulated by incorporating acid-catalyzed cross-linking chemistry. The SEM images of one such 157-nm bilayer resist are shown in Fig. **c**. This multilayer approach does require additional coating and etch steps, and for this reason has not yet achieved widespread use in semiconductor manufacturing.

Extreme Ultraviolet Lithography. This lithographic technology was first proposed as a candidate for the production of semiconductors in 1988 . It is a form of step- and scan-projection lithography using a plasma radiation source that emits soft X-rays in the 10–14-nm wavelength range. This technology can be viewed as an evolutionary extension of the duv optical imaging techniques described earlier. The principal differences are consequences of the energy of the exposing light. In the soft X-ray region, essentially all materials are strong absorbers. Because of this, the reduction optics employed in euv exposure systems are based on multilayer mirrors and reflective masks enclosed in a high

vacuum. The fabrication of these optical components must be carried out to ultra-precise tolerances and is a significant challenge.

The absorption of radiation at these wavelengths is a direct function of the atomic composition and density of the material, so the transmission characteristics of a resist film can be simply calculated from the mass absorption coefficients and percentages of each element that comprise the film . Unlike duv resists, the nature of carbon–carbon bonding in the polymer has only a minor effect on absorption. At euv wavelengths, phenolic-based CA resists have absorbances on the order of 3–5/μ thickness , and currently are used as very thin single-layer resists, often in conjunction with a hard mask: a thin layer of a material that can be etched with a specific plasma chemistry, but that then acts as an effective etch barrier during transfer of the pattern to substrate. The replacement of carbon with lighter elements, such as boron, will lead to a more transparent polymer, and bilayer resists containing boron have been described for euv applications .

Most of the euv light sources currently under development, laser induced plasmas, and gas discharge plasmas, are inefficient sources of soft X-rays. In consequence, very sensitive photoresists will be required. Throughput calculations indicate that a resist exposure dose on the order of 5 mJ/cm^2 will be required to achieve acceptable, cost-effective wafer throughput for these expensive exposure systems. The low dose specification, combined with the high energy nature of euv radiation, raises the potential that shot-noise effects will lead to poor dimensional control. In addition, several studies of euv resists have shown an apparent increase in line edge roughness as the resist photospeed decreases . All of these challenges need to be addressed if euv is to be implemented as a mainstream manufacturing technology.

Current thinking is that euv lithography will find first use for the 32-nm device generation and beyond. Therefore, the resolution requirements for euv resists are extremely demanding and may approach the limits of CA resist technology. Experimental CA resists have been used to resolve features as small as 25–30 nm using euv lithography, albeit with less than optimal profile control and large LER (Fig.) .

6. Lithography Without Imaging Radiation

Recently, several new lithographic fabrication techniques have been developed that rely on mechanical pattern transfer and, as such, are distinctly different from the photoresist-based procedures we have discussed up to this point. These methods are adapted from familiar manufacturing processes, such as contact printing, molding and embossing, and have been modified to produce patterns with features < 100 nm . The low cost and versatility of the technologies have led to their use in a range of different applications, and there is currently significant interest in developing a least one of these techniques for semiconductor manufacturing. The three most widely used of these techniques are described in the following sections.

6.1. Microcontact Printing (μμCP). This technique, a form of so-called "soft lithography" (Fig. **a**), employs a compliant elastomeric stamp and a hydrophobic "ink" to print patterns on suitable substrate . Resolution at the submicron scale has been demonstrated. Long-chain alkane thiols, of the generic structure $(CH_3{-}(CH_2)_n{-}SH$, form self-assembled monolayers (SAMs) on surfaces such as gold and have been widely use as μCP inks . Once patterned by stamping, the SAM can then serve as a mask for subsequent pattern transfer into the gold layer by wet etch techniques. Stamps are usually formed from polymers, such as poly(dimethylsiloxane), on a rigid mold. Typically, the molds are made using electron-beam or optical lithography. Stamps with features on the order of 50–80 nm can be fabricated in this fashion . Recently, elastomeric stamps with 2-nm features have been prepared using carbon nanotube-based masters . Pictures of an elastomeric stamp and a patterned gold substrate are shown in Fig. .

Microcontact printing has seen use in a variety of applications, including the fabrication of structures on nonplanar surfaces , the direct, high resolution printing of arrays of biological molecules , and the construction of nanowire arrays . The use of soft stamps in semiconductor applications is problematic, however. Defects, feature distortion, and alignment issues are serious concerns when using elastomeric stamps. There have been attempts to minimize such deformations using partially hardened stamps . The use of gold substrates, monolayer resists, and wet etch processes also pose problems for semiconductor processing.

6.2. Nanoembossing. Nanoembossing is a contact printing method, where a rigid mold stamps a relief pattern into a heated, deformable surface that is then cooled and made rigid before removing the stamp (Fig. **b**). Typically, the deformable surface is a spin-cast film of a polymer, such as PMMA, and is heated to a temperature near its T_g. These are used with metal stamps fabricated by conventional photolithography. The final relief image can serve as an etch mask, just like a developed photoresist pattern. However, the forming process does not bring the stamp into direct contact with the substrate, so there remains a thin residual layer in the embossed areas that must be etched through before pattern transfer to the substrate can be carried out. Features as small as 5 nm have been printed in polymer substrates . A variety of polymers have been used as the transfer medium. Recently, the direct patterning of laser heated silicon

substrates has been reported . The thermal processing at elevated temperature raises concerns about pattern placement and fidelity; nonetheless, functional semiconductor devices have been fabricated using this technique . Several commercial vendors are supplying this technology.

6.3. Optical Nanoimprinting. This technique (Fig. **c**), also known as step and flash imprint lithography, currently is considered to offer the best opportunity among the contact-based approaches to compete with or even replace semiconductor photolithography. A liquid polymer precursor is dispensed or coated onto a suitable substrate, contacted with a transparent quartz stamp or mold, and irradiated to photopolymerize the precursor prior to separating substrate from mold. The low viscosity fluid resists, typically acrylate monomers, readily fill the transparent mold and enable easy alignment, since they allow the stamp to be moved while in contact with the fluid. This is a significant advantage compared to the thermal nanoembossing approach. The resist liquid can be dispensed by inkjet techniques that minimize material waste and can reduce printing nonuniformities that stem from pattern density differences across the stamp.

The photopolymerization chemistry is similar to that used in the manufacture of printed circuit boards , and early versions of the compact disk . Photocuring produces a relief pattern similar to that generated by nanoembossing (Fig.). If silyl acrylates are used as the printing medium and coated atop a thick organic polymer underlayer, then the patterned silicon-based polymer can be used as a high selectivity etch mask in an oxygen RIE step to form a final etch resistant mask for substrate etching (Fig.). This is analogous to the bilayer process described earlier for 157-nm applications.

When compared with photolithography, this technique has potential advantages in resolution (it is not diffraction limited, and LER issues are expected to be of concern only during fabrication of the stamp), cost (expensive optical exposure systems, complex masks and expensive photoresists are not required), and simplicity (reflectivity control and depth of focus are not considerations). Many of the issues that must be resolved in the practical implementation of this technology relate to the stamp. Fabricating defect-free masks with 30-nm dimensions is a significant challenge, even with state-of-the-art e-beam lithography tooling and processes. Defect generation and mask damage during contact printing are concerns, and a means for repair of the transparent masks in 3D will be required. These issues are now under active investigation and as of early 2005 optical nanoimprinting is listed in the current ITRS as a candidate for 32-nm technology node.

Bibliography

"Lithographic Resists" in *ECT* 4th ed., Suppl. Vol., pp. 233–280, by W. D. Hinsberg, G. M. Wallraff, and R. D. Allen, IBM Research Division; "Lithographic Resists" in *ECT* (online), posting date: December 4, 2000, by W. D. Hinsberg, G. M. Wallraff, and R. D. Allen, IBM Research Division.

7. C. G. Willson, L. Thompson, and M. Bowden, eds., *Introduction to Microlithography*, 2nd ed., American Chemical Society, Washington, D.C., 1994.

8. W. Moreau, *Semiconductor Lithography*, Plenum Press, New York, 1988.
9. E. Reichmanis and A. Novembre, *Ann. Rev. Mater. Sci.* **23**, 11 (1993).
10. J. Shaw and co-workers, *J. Vac. Sci. Tech. B* **7**(6), 1709 (1989).
11. G. Moore, *Proc. Soc. Photo-Opt. Instr. Eng.* **2438**, 2 (1995).
12. J. Bryzek, K. Pedersen, and W. McCulley, *IEEE Spectrum* **31**(5), 20 (1994).
13. P. Rai-Choudhury, ed., *Handbook of Microlithography, Micromachining and Microfabrication*, Vol. 2, SPIE-International Society for Optical Engineers, Bellingham Wash., 1997.
14. L. Lin, S. Lee, K. Pister, and M. Wu, *IEEE Photonics Technol. Lett.* **6**, 1445 (1994) and references cited therein.
15. D. Cho and co-workers, eds., *Micromechanical Sensors, Actuators and Systems*, American Society of Mechanical Engineers, New York, 1991.
16. M. Eggers and D. Ehrlich, *Hematolog. Pathol.* **9**(1), 1 (1995).
17. W. DeForest, *Photoresist: Materials and Processes*, McGraw-Hill, New York, 1975.
18. P. Hartsuch, *Chemistry of Lithography*, Lithographic Technical Foundation, New York, 1961.
19. G. Mannivannan, R. Changkakoti, R. Lessard, G. Mailhot, and M. Bolte, *J. Phys. Chem.* **97**, 7228 (1993).
20. L. F. Thompson and R. E. Kerwin, *Ann. Rev. Matls. Sci.* **6**, 267 (1976).
21. M. King, in N. Einspruch, eds., *VLSI Electronics: Microstructure Science*, Vol. 1, Academic Press, New York, 1981, Chapt. 2.
22. M. Gurian and N. Ivory, *Electronic Packag. Prod.* **35**(3), 49 (1995).
23. S. Baller, *Printed Circuit Fab.* **18**(7), 28 (1995).
24. H. Pfeiffer, *Solid State Technol.* **27**(9), 223 (1984).
25. J. Warlaumont, *J. Vac. Sci. Tech. B* **7**(6), 1634 (1989).
26. J. Lingnau, R. Dammel, and J. Theis, *Solid State Technol.* **32**(9), 105 (1989).
27. J. Lingnau, R. Dammel, and J. Theis, *Solid State Technol.* **32**(10), 107 (1989).
28. L. Thompson and M. Bowden, *J. Electrochem. Soc.* **120**, 1722 (1973).
29. M. McCoy, *Chem. Eng. News* **82**, 18 (2004).
30. R. Dammel, *Diazonaphthoquinone-based Resists*, SPIE Optical Engineering Press, Bellingham, Wash., 1993.
31. F. Billmeyer, *Textbook of Polymer Science*, 2nd ed., Wiley-Interscience, New York, 1984, pp. 436–439.
32. P. Trefonas and B. Daniels, *Proc. Soc. Photo-Opt. Instr. Eng.* **771**, 194 (1987).
33. C. Szmanda, A. Zampini, D. Madoux, and C. McCants, *Proc. Soc. Photo-Opt. Instr. Eng.* **1086**, 363 (1989).
34. S. Kishimura, A. Yamaguchi, Y. Yamada, and H. Nagata, *Polym. Eng. Sci.* **32**(20), 1550 (1992).
35. K. Uenishi, Y. Kawabe, T. Kokubo, S. Slater, and A. Blakeney, *Proc. Soc. Photo-Opt. Instr. Eng.* **1466**, 102 (1991).
36. K. Honda, B. Beauchemin, R. Hurditch, A. Blakeney, Y. Kawabe, and T. Kobuko, *Proc. Soc. Photo-Opt. Instr. Eng.* **1262**, 493 (1990).
37. M. Hanabata, Y. Uetani, and A. Furuta, *J. Vac. Sci. Tech. B* **7**(4), 640 (1989).
38. M. Hanabata, F. Oi, and A. Furuta, *Proc. Soc. Photo-Opt. Instr. Eng.* **1466**, 132 (1991).
39. M. Lepselter and W. Lynch, in Ref. , Chapt. 3.
40. G. Pawlowski and co-workers, *Proc. Soc. Photo-Opt. Instr. Eng.* **1262**, 391 (1990).
41. H. Ito and G. Wilson, *Polym. Eng. Sci.* **23**, 1012 (1982).
42. J. Frechet, H. Ito, and C. G. Willson, *Proc. Microcircuit Eng.* **82**, 260 (1982).
43. D. McKean, U. Schaedili, and S. MacDonald, in E. Reichmanis, S. MacDonald, and T. Iwayanagi, eds., *Polymers in Microlithography, ACS Symposium Series 412*, American Chemical Society, Washington, D.C., 1989, pp. 27–38.

44. J. Maltabes and co-workers, *Proc. Soc. Photo-Opt. Instr. Eng.* **1262**, 2 (1990).
45. E. Reichmanis, F. Houlihan, O. Nalamasu, and T. Neenan, *Chem. Matls.* **3**, 394 (1991).
46. J. Crivello, in J. P. Fouiassier and J. F. Rabek, eds., *Radiation Curing in Polymer Science and Technology (Vol II): Photoinitiating Systems*, Elsevier, New York, 1993, Chapt. 8, for a review on onium salts.
47. H. Ito and G. Willson, in T. Davidson, ed., *Polymers in Electronics, ACS Symposium Series 242*, American Chemical Society, Washington, D.C., 1984, pp. 11–24.
48. R. Allen, G. Wallraff, W. Hinsberg, L. Simpson, and R. Kunz, *Polymers for Microelectronics, ACS Symposium Series 537*, American Chemical Society, Washington, D.C., 1994, p. 165.
49. K. Nakano, K. Maeda, S. Iwasa, T. Ohfuji, and E. Hasegawa, *Proc. Soc. Photo-Opt. Instr. Eng.* **2438**, 433 (1995).
50. F. Saeva, D. Breslin, and H. Luss, *J. Am. Chem. Soc.* **113**, 5333 (1991).
51. M. F. Cronin, T. Adams, T. Fedynyshyn, J. Georger, J. Michael Mori, R. Sinta, and J. W. Thackeray, *Proc. Soc. Photo-Opt. Instr. Eng.* **2195**, 214 (1994).
52. J. March, *Advanced Organic Chemistry*, 4th ed., Wiley-Interscience, New York, 1992, p. 250.
53. D. McKean, R. Allen, P. Kasai, U. Schaedili, and S. MacDonald, *Proc. Soc. Photo-Opt. Instr. Eng.* **1672**, 94 (1992).
54. H. Ito, *Proc. Soc. Photo-Opt. Instr. Eng.* **920**, 33 (1988).
55. G. Wallraff, R. Allen, W. Hinsberg, L. Simpson, and R. Kunz, *Chemtech* **23**(4), 22 (1993).
56. N. Hacker, in J. P. Fouiassier and J. F. Rabek, eds., *Radiation Curing in Polymer Science and Technology*, Vol. II, *Photoinitiating Systems*, Elsevier, New York, 1993, Chapt. 9.
57. R. DeVoe, M. Sahyun, and E. Schmidt, *Can. J. Chem.* **66**, 319 (1988).
58. R. Binkley and T. Flechtner, in W. Horspool, ed., *Synthetic Organic Photochemistry*, Plenum Press, New York, 1984, Chapt. 7.
59. T. Neenan and co-workers, *Macromolecules* **23**, 145 (1990).
60. N. Hayashi, L. Schlegel, T. Ueno, H. Shiraishi, and T. Iwayanagi, *Proc. Soc. Photo-Opt. Instr. Eng.* **1466**, 377 (1991).
61. L. Schlegel, T. Ueno, H. Shiraishi, N. Hayashi, and T. Iwayanagi, *Chem. Mater.* **2**, 299 (1990).
62. K. Naitoh, K. Yoneyma, and T. Yamaoka, *J. Phys. Chem.* **96**, 238 (1992).
63. H. Ito, G. Breyta, D. Hofer, T. Fischer, and B. Prime, *Proc. Soc. Photo-Opt. Instr. Eng.* **2438**, 53 (1995).
64. G. Buhr, H. Lenz, and S. Scheler, *Proc. Soc. Photo-Opt. Instr. Eng.* **1086**, 117 (1989).
65. M. Shirai and M. Tsunooka, *Progr. Polym. Sci.* **21**, 1–45 (1996).
66. T. H. Lowery and K. S. Richardson, *Mechanism and Theory in Organic Chemistry*, 3rd ed., Harper and Row, New York, 1987, Chapt. 7.
67. Ref. , Table 10.14, p. 380.
68. D. McKean, S. MacDonald, N. Clecak, and G. Willson, *Proc. Soc. Photo-Opt. Instr. Eng.* **1925**, 246 (1993).
69. R. Allen and co-workers, *Proc. Soc. Photo-Opt. Instr. Eng.* **1925**, 246 (1993).
70. H. Ito, M. Ueda, and R. Schwalm, *J. Vac. Sci. Technol. B* **6**, 2259 (1988).
71. D. Funhoff, H. Binder, and R. Schwalm, *Proc. Soc. Photo-Opt. Instr. Eng.* **1672**, 46 (1992).
72. R. Allen, W. Conley, and J. Gelorme, *Proc. Soc. Photo-Opt. Instr. Eng.* **1672**, 513 (1992).
73. W. Feeley, J. Imhof, and C. Stein, *Polym. Eng. Sci.* **26**, 1101 (1986).

74. J. Frechet, S. Matsuszczak, H. Stover, C. Willson, and B. Reck, in E. Reichmanis, S. A. MacDonald, and T. Iwayanagi, eds., *Polymers in Microlithography, ACS Symposium Series 412*, American Chemical Society, Washington, D.C., 1989, p. 74.
75. G. Wallraff and co-workers, *J. Vac. Sci. Technol. B* **12**, 3857 (1994).
76. S. Holmes and J. Sturtevant, *Microlithog. World* **2**, 17 (1993).
77. W. Conley and co-workers, *Proc. Soc. Photo-Opt. Instr. Eng.* **3049**, 282 (1997).
78. U. Kumar, A. Pandya, R. Sinta, W. Huang, R. Bantu, and A. Katnani, *Proc. Soc. Photo-Opt. Instr. Eng.* **3049**, 135 (1997).
79. G. M. Wallraff, J. Hutchinson, W. Hinsberg, F. Houle, and P. Seidel, *Microelectronic Eng.* **27**, 397 (1995).
80. W. Huang, R. Kwong, A. Katani, and M. Khojasteh, *Proc. Soc. Photo-Opt. Instr. Eng.* **2195**, 37 (1994).
81. K. Przybilla and co-workers, *Proc. Soc. Photo-Opt. Instr. Eng.* **1925**, 76 (1993).
82. T. Hattori, A. Imai, R. Yamanaka, T. Ueno, and H. Shiraishi, *J. Photopolym. Sci. Technol.* **9**, 611 (1996).
83. S. MacDonald and co-workers, *Proc. Soc. Photo-Opt. Instr. Eng.* **1466**, 1 (1991).
84. O. Nalamasu and co-workers, *Proc. Soc. Photo-Opt. Instr. Eng.* **1466**, 13 (1991).
85. R. Cox, L. Druet, A. Klausner, T. Modro, P. Wan, and K. Yates, *Can. J. Chem.* **59**, 1568 (1981).
86. A. Oikawa and co-workers, *Proc. Soc. Photo-Opt. Instr. Eng.* **2438**, 599 (1995).
87. T. Kumeda and co-workers, *Proc. Soc. Photo-Opt. Instr. Eng.* **1925**, 31 (1993).
88. A. Oikawa, N. Santoh, S. Miyata, and Y. Hatakenaka, *Proc. Soc. Photo-Opt. Instr. Eng.* **1925**, 92 (1993).
89. Y. Kawai, A. Otaka, A. Tanaka, and T. Matsuda, *Jpn. J. Appl. Phys.* **33**, 7023 (1994).
90. Y. Kawai, A. Otaka, J. Nakamura, A. Tanaka, and T. Matsuda, *J. Photopolym. Sci. Techn.* **8**, 535 (1995).
91. K. Asakawa, T. Ushirogouchi, and M. Nakase, *Proc. Soc. Photo-Opt. Instr. Eng.* **2438**, 563 (1995).
92. S. Satio and co-workers, *J. Photopolym. Sci. Technol.* **9**, 677 (1996).
93. W. Hinsberg, S. MacDonald, N. Clecak, and C. Snyder, *Proc. Soc. Photo-Opt. Instr. Eng.* **1672**, 24 (1992).
94. W. Hinsberg, S. MacDonald, N. Clecak, C. Snyder, and H. Ito, *Proc. Soc. Photo-Opt. Instr. Eng.* **1925**, 43 (1993).
95. P. Paniez, C. Rosilio, B. Mouanda, and F. Vinet, *Proc. Soc. Photo-Opt. Instr. Eng.* **2195**, 14 (1994).
96. H. Ito and co-workers, *Proc. Soc. Photo-Opt. Instr. Eng.* **1925**, 65 (1993).
97. G. Breyta and co-workers, *J. Photopolym. Sci. Tech.* **7**, 449 (1994).
98. J. E. McGrath, *J. Chem. Ed.* **58**(11), 844 (1981).
99. H. Gokan, S. Esho, and Y. Ohnishi, *J. Electrochem. Soc.* **130**, 143 (1983).
100. R. Kunz and co-workers, *Proc. Soc. Photo-Opt. Instr. Eng.* **2724**, 365 (1996).
101. T. Wallow and co-workers, *Proc. Soc. Photo-Opt. Instr. Eng.* **3333**, 92 (1998).
102. R. Allen, G. Wallraff, R. DiPietro, D. Hofer, and R. Kunz, *Proc. Soc. Photo-Opt. Instr. Eng.* **2438**, 474 (1995).
103. H. Ito, N. Seehof, R. Sato, T. Nakayama, and M. Ueda, *Micro- and Nano-Patterning Polymers, ACS Symposium Series 706*, in H. Ito, E. Reichmanis, O. Nalamasu, and T. Ueno, eds., American Chemical Society, Washington, D.C., 1998, p. 208.
104. K. Patel and co-workers, *Proc. Soc. Photo-Opt. Instr. Eng.* **5376**, 94 (2004).
105. K. Przybilla, H. Roeschert, and G. Pawlowski, *Proc. Soc. Photo-Opt. Instr. Eng.* **1672**, 500 (1992).
106. R. Kunz, R. Allen, W. Hinsberg, and G. Wallraff, *Proc. Soc. Photo-Opt. Instr. Eng.* **1925**, 167 (1993).

107. Y. Kaimoto, K. Nozaki, S. Takechi, and N. Abe, *Proc. Soc. Photo-Opt. Instr. Eng.* **1672**, 66 (1992).
108. M. Takahashi and co-workers, *Proc. Soc. Photo-Opt. Instr. Eng.* **2438**, 422 (1995).
109. K. Nozaki and co-workers, *J. Photopolym. Sci. Techn.* **9**, 509 (1996).
110. N. Shida, T. Oshirogouchi, K. Asakawa, and N. Nakase, *J. Photopolym. Sci. Techn.* **9**, 457 (1996).
111. M. Padmanaban and co-workers, *J. Photopolym. Sci. Techn.* **13**, 607 (2000).
112. R. Allen and co-workers, *Proc. Soc. Photo-Opt. Instr. Eng.* **2724**, 334 (1996).
113. U. Okoroanyanwu, J. Byers, T. Shimokawa, and G. Willson, *Chem. Matls.* **10**, 3328 (1998).
114. U. Okoroanyanwu, T. Shimokawa, J. Byers, and G. Willson, *Chem. Matls.* **10**, 3319 (1998).
115. H. Ito and co-workers, *Proc. Soc. Photo-Opt. Instr. Eng.* **3999**, 2 (2000).
116. H. Ito and co-workers, *Proc. Soc. Photo-Opt. Instr. Eng.* **3999**, 2 (2000).
117. T. Wallow and co-workers, *Proc. Soc. Photo-Opt. Instr. Eng.* **2724**, 355 (1996).
118. J. Jung, C. Bok, and K. Baik, *Proc. Soc. Photo-Opt. Instr. Eng.* **3333**, 11 (1998).
119. F. Houlihan and co-workers, *Proc. Soc. Photo-Opt. Instr. Eng.* **3049**, 84 (1997).
120. S. Choi, H. Kim, S. Woo, and J. Moon, *Proc. Soc. Photo-Opt. Instr. Eng.* **3999**, 54 (2000).
121. International Technical Roadmap for Semiconductors, SEMATECH, Inc., Austin, Tex., updated 2004.
122. G. Castellan, *Physical Chemistry*, 2nd ed., Addison-Wesley, Reading, Mass., 1971, p. 578.
123. A. Broers, A. Hoole, and J. Ryan, *Microelectron. Eng.* **32**, 131 (1996).
124. A. Broers, *J. Electrochem. Soc.* **128**, 166 (1981).
125. C. Vieu and co-workers, *Appl. Surf. Sci.* **164**, 111 (2000).
126. S. Yasin, D. Hasko, and H. Ahmed, *Microelectron. Eng.* **61–62**, 745 (2002).
127. W. Chen and H. Ahmed, *Appl. Phys. Lett.* **62**, 1499 (1993).
128. I. Haller, M. Hatzakis, and R. Srinivasan, *IBM J. Res. Devel.* **12**, 251 (1968).
129. C. Umbach, A. Broers, G. Willson, R. Koch, and R. Laibowitz, *J. Vac. Sci. Techn. B* **6**, 319 (1988).
130. J. T. Everhart, *Materials for Microlithography*, in L. Thompson, G. Willson, and J. Frechet, eds., American Chemical Society Symposium Series 266, 1984; Chapt. 1.
131. Nakamura, H. Ban, K. Deguchi, and A. Tanaka, *Jpn. J. Appl. Phys. Part 1* **30**, 2619 (1991).
132. L. Schlegel, T. Ueno, N. Hayashi, and T. Iwayanagi, *J. Vac. Sci. Techn. B* **9**, 278 (1991).
133. J. Thackeray and co-workers, *J. Photopolym. Sci. Technol.* **3**, 619 (1994).
134. T. Itani and co-workers, *Jpn. J. Appl. Phys. Part 1* **35**, 6501 (1996).
135. S. Postnikov and co-workers, *J. Vac. Sci. Techn. B* **17**, 3335 (1999).
136. F. Houle and co-workers, *J. Vac. Sci. Techn. B* **18**, 1874 (2000).
137. K. Asakawa, T. Ushiogouchi, and M. Nakase, *Proc. Soc. Photo-Opt. Instr. Eng.* **2438**, 563 (1995).
138. S. Saito and co-workers, *J. Photopolym. Sci. Technol.* **9**, 677 (1996).
139. W. Hinsberg and co-workers, *Proc. Soc. Photo-Opt. Instr. Eng.* **3999**, 148 (2000).
140. W. Hinsberg and co-workers, *Proc. Soc. Photo-Opt. Instr. Eng.* **5039**, 1 (2003).
141. G. Wallraff and co-workers, *J. Vac. Sci. Technol. B* **22**, 3479 (2004).
142. J. Hutchinson and co-workers, *Proc. Soc. Photo-Opt. Instr. Eng.* **3333**, 165 (1998).
143. E. Shiobara and co-workers, *Proc. Soc. Photo-Opt. Instr. Eng.* **3333**, 313 (1998).
144. T. Yoshimura, H. Shiaishis, J. Yamamoto, and S. Okazaki, *Jpn. J. Appl. Phys.* **32**, 6065 (1993).

145. J. Yamamoto, S. Uchino, T. Hattori, T. Yoshimura, and F. Murai, *Jpn. J. Appl. Phys.* **35**, 6511 (1996).
146. M. Sanchez, W. Hinsberg, F. Houle, J. Hoffnagle, H. Ito, and C. Nguyen, *Proc. Soc. Photo-Opt. Instr. Eng.* **3678**, 160 (1999).
147. L. Flanagin, V. Singh, and G. Willson, *J.Vac. Sci Techn. B* **17**, 1371 (1999).
148. F. Houle, W. Hinsberg, and M. Sanchez, *Macromol.* **35**, 8591 (2002).
149. T. Ushirogouchi, K. Asakawa, M. Nakase, and A. Hongu, *Proc. Soc. Photo-Opt. Instr. Eng.* **2438**, 609 (1995).
150. M. Rooks and A. Aviram, *J. Vac. Sci. Technol. B* **17**, 3394 (1999).
151. A. Robinson and co-workers, *J. Phys. D: Appl. Phys.* **32**, L75 (1999).
152. T. Tanaka, M. Morigumi, and N. Atoda, *Jpn. J. Appl. Phys. Part 1* **32**, 6059 (1993).
153. H. Cao, P. Nealey, and W. Domke, *J. Vac. Sci. Technol. B* **18**, 3303 (2000).
154. H. Namatsu, K. Yamazaki, and K. Kurihara, *Microelectron. Eng.* **46**, 129 (1999).
155. S. Turner, C. Babcock, and F. Cerrina, *J. Vac. Sci.Techn. B* **9**, 3440 (1991).
156. A. Neureuther and G. Willson, *J. Vac. Sci. Techn. B* **6**, 167 (1988).
157. N. Rau and co-workers, *J. Vac. Sci.Techn. B* **16**, 3784 (1998).
158. W. Brunger and co-workers, *J. Vac. Sci. Techn. B* **17**, 3119 (1999).
159. D. He, H. Solak, W. Li, and F. Cerrina, *J. Vac. Sci. Techn. B* **17**, 3779 (1999).
160. S. O'Brien and M. Mason, *Proc. Soc. Photo-Opt. Instr. Eng.* **4346**, 534 (2001).
161. P. Dentinger and co-workers, *J. Vac. Sci. Techn. B* **17**, 3779 (1999).
162. G. Gallatin, *Proc. Soc. Photo-Opt. Instr. Eng.* **4404**, 123 (2001).
163. M. Wilson and co-workers, *IBM J. Res. Develop.* **37**, 357 (1993).
164. B. Boerger and co-workers, *Proc. Soc. Photo-Opt. Instr. Eng.* **5037**, 1112 (2003).
165. Y. Nakayama, S. Okazaki, N. Saitou, and H. Wakabayashi, *J. Vac. Sci. Technol. B* **8**, 1836 (1990).
166. L. R. Harriott and co-workers, *J. Vac. Sci. Technol. B* **14**, 3825 (1996).
167. L. Murray and co-workers, *J. Vac. Sci. Technol. B* **18**, 3099 (2000).
168. H. Loschner and co-workers, *J. Vac. Sci. Technol. B* **11**, 487 (1993).
169. C. V. Shank and R. V. Schmidt, *Appl. Phys. Lett.* **23**, 154 (1973).
170. B. Lin, *Microelectron. Eng.* **6**, 31 (1987).
171. B. Lin, *J. Microlith. Microfab. Microsys.* **3**, 377 (2004).
172. J. Mulkens, D. Flagelo, B. Streefkerk, and P. Graeupner, *J. Microlith. Microfab. Microsys.* **3**, 104 (2004).
173. B. Smith and co-workers, *J. Microlith., Microfab. Microsyst.* **3**, 44 (2004).
174. W. Hinsberg and co-workers, *Proc. Soc. Photo-Opt. Instr. Eng.* **5376**, 21 (2004).
175. A. K. Raub and co-workers, *J. Vac. Sci Techn. B* **22**, 3459 (2004).
176. D. Henderson, J. White, H. Craighead, and I. Adesida, *Appl. Phys. Lett.* **46**, 900 (1985).
177. T. Bloomstein and co-workers, *J. Vac. Sci. Techn. B* **15**, 2112 (1997).
178. J. Burnett, R. Gupta, and U. Griesmann, *Proc. Soc. Photo-Opt. Instr. Eng.* **4000**, 1503 (2000).
179. A. Grenville and co-workers, *Proc. Soc. Photo-Opt. Instr. Eng.* **4691**, 1644 (2002).
180. C. Sandorfy and L. Lussier, *Photophysics and Photochemistry in the Vacuum Ultraviolet*, in S. McGlynn and R. Huebner, eds., D. Reidel Publishing, Dordrecht, The Netherlands, 1985, p. 819.
181. M. Robin, *Higher Excited States of Organic Molecules*, Vols. I–III Academic Press, New York, 1974.
182. R. Kunz and co-workers, *Proc. Soc. Photo-Opt. Instr. Eng.* **16**, 3678 (1999).
183. R. Kunz and co-workers, *J. Vac. Sci. Technol B* **16**, 3267 (1999).
184. Ref. , Vol. I Chapt. 3.
185. S. Kishimura, M. Endo, and M. Sasago, *Proc. Soc. Photo-Opt. Instr. Eng.* **200**, 4690 (2002).

186. Y. Kawaguchi and co-workers, *Proc. Soc. Photo-Opt. Instr. Eng.* **5039**, 43 (2003).
187. C. Chambers and co-workers, *Proc. Soc. Photo-Opt. Instr. Eng.* **5376**, 360 (2004).
188. A. Hamad, F. Houlihan, L. Seger, C. Chang, and C. Ober, *Proc. Soc. Photo-Opt. Instr. Eng.* **5039**, 558 (2003).
189. T. Ishikawa and co-workers, *J. Photopolym. Sci. Technol.* **17**, 631 (2004).
190. H. Ito and co-workers, *J. Photopolym. Sci. Technol.* **17**, 609 (2004).
191. B. Trinque and co-workers, *Proc. Soc. Photo-Opt. Instr. Eng.* **4690**, 58 (2002).
192. T. Sasaki and co-workers, *J. Photopolym. Sci. Technol.* **17**, 639 (2004).
193. R. Miller and G. Wallraff, *Adv. Mat. Opt. Electron.* **4**, 95 (1994).
194. T. Furukawa and co-workers, *Proc. Soc. Photo-Opt. Instr. Eng.* **5367**, 1064 (2004).
195. A. Hawryluk and L. Seppala, *J. Vac. Sci. Technol. B* **6**, 2162 (1988).
196. M. J. Bowden, in Ref. , Chapt. 2.
197. B. Henke, E. Gullikson, and J. Davis, *Atomic Data Nuclear Data Tables* **54**, 181 (1993).
198. M. Chandhok and co-workers, *Proc. Soc. Photo-Opt. Instr. Eng.* **5374**, 861 (2004).
199. H. Cao and co-workers, *Proc. Soc. Photo-Opt. Instr. Eng.* **5039**, 485 (2003).
200. J. Dai and C. Ober, *Proc. Soc. Photo-Opt. Instr. Eng.* **5376**, 508 (2004).
201. R. Brainard and co-workers, *Proc. Soc. Photo-Opt. Instr. Eng.* **5374**, 74 (2004).
202. P. Naulleau and co-workers, *J. Vac. Sci. Technol. B* **22**, 2962 (2004).
203. B. Gates and co-workers, *Chem. Rev.* **105**, 1171 (2005).
204. Y. Xia and G. Whitesides, *Angew. Chem. Int. Ed. Engle* **37**, 550 (1998).
205. B. Michel and co-workers, *IBM J. Res. Dev.* **45**, 697 (2001).
206. H. Schmid and B. Michel, *Macromol.* **33**, 3042 (2000).
207. F. Hua and co-workers, *Nano Lett.* **4**, 2467 (2004).
208. J. Rogers, *Matls. Res. Soc.Proc.* **739**, 31 (2002).
209. H. James and co-workers, *Langmuir* **14**, 741 (1998).
210. E. Delamarche, *Nanobiotechnology: Concepts, Applicationa and Perspectives*, in C. Niemeyer and C. Mirkin, eds., John Wiley & Sons Inc., Hoboken, N.J., 2004, Chapt. 3.
211. Y. Sun and J. Rogers, *Nano Lett.* **4**, 1953 (2004).
212. T. Odom, J. Love, D. Wolfe, K. Paul, and G. Whitesides, *Langmuir* **18**, 5314 (2002).
213. K. Choi and J. Rogers, *Matls. Res. Soc.Proc.* **820**, 147 (2004).
214. S. Chou, P. Krauss, and P. Renstrom, *Science* **272**, 5258 (1996).
215. S. Chou, P. Krauss, W. Zhang, L. Guo, and L. Zhuang, *J. Vac. Sci.Technol. B* **15**, 2897 (1997).
216. S. Chou, C. Keimel, and J. Gu, *Nature (London)* **417**, 835 (2002).
217. W. Zhang and S. Chou, *Appl. Phys. Lett.* **83**, 1632 (2003).
218. D. Resnick, S. Sreenivasan, and G. Willson, *Mat. Today* **8**, 34 (2005).
219. D. Resnick and co-workers, *Proc. Soc. Photo-Opt. Instr. Eng.* **5037**, 12 (2003).
220. H. Haverkorn van Rijsewijk, P. Legierse, and G. Thomas, *Philips Tech. Rev.* **40**, 287 (1982).

W. D. HINSBERG
G. M. WALLRAFF
IBM Research Division

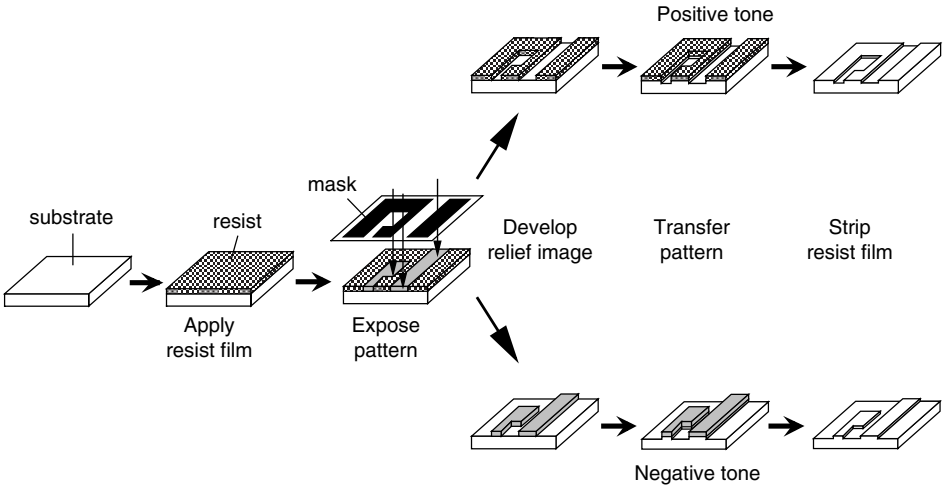

Fig. 1. The lithographic process. A substrate is coated with a photosensitive polymer film called a resist. A mask with transparent and opaque areas directs radiation to preselected regions of the resist film. Depending on resist characteristics, exposed or unexposed portions of the film are removed using a developer solvent. The resulting pattern is then transferred to the substrate surface and the resist is stripped.

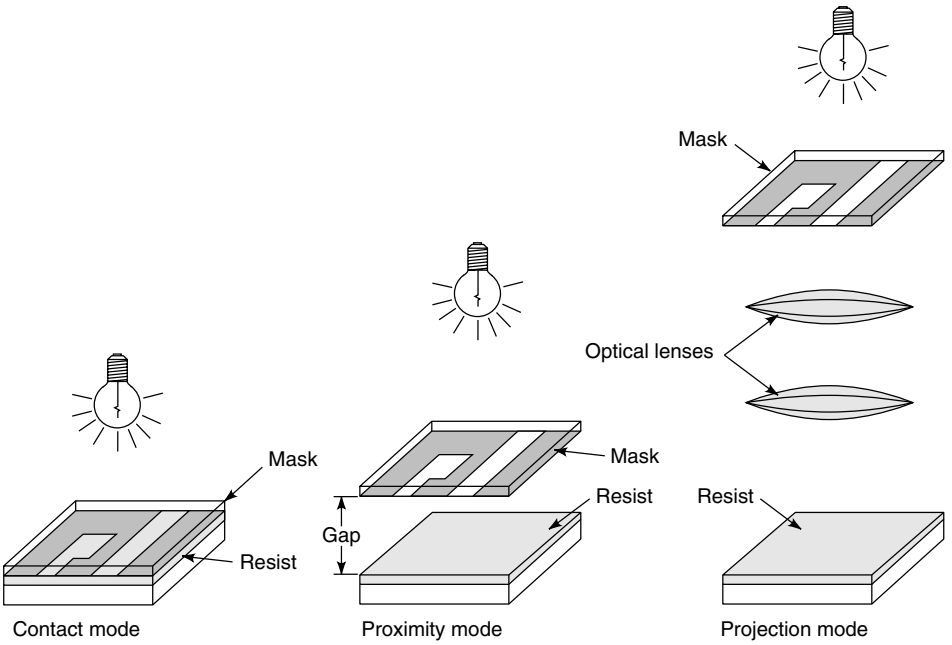

Fig. 2. Contact, proximity, and projection modes of optical lithography. Although contact mode generally produces the sharpest light image, damage to mask and substrate make this impractical for most electronic device applications. In proximity mode, a narrow, uniform gap between mask and substrate minimizes damage, but blurs the light image. Using projection mode, the light image is transmitted through a sophisticated system of high quality optical lenses, delivering a sharper light image than can be attained in proximity mode .

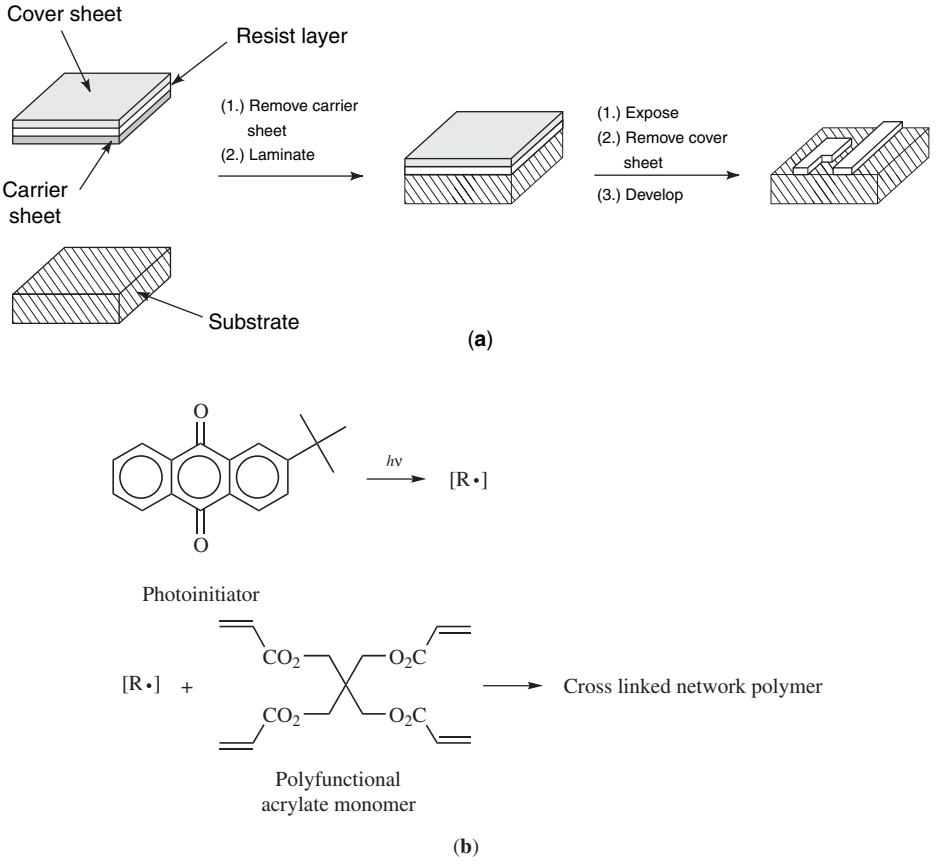

Fig. 3. Chemistry of a dry-film, negative-acting photoresist. (**a**) Polymerizable layer sandwiched between a polyolefin carrier sheet and a polyester cover sheet. (**b**) Chemical structures of typical components.

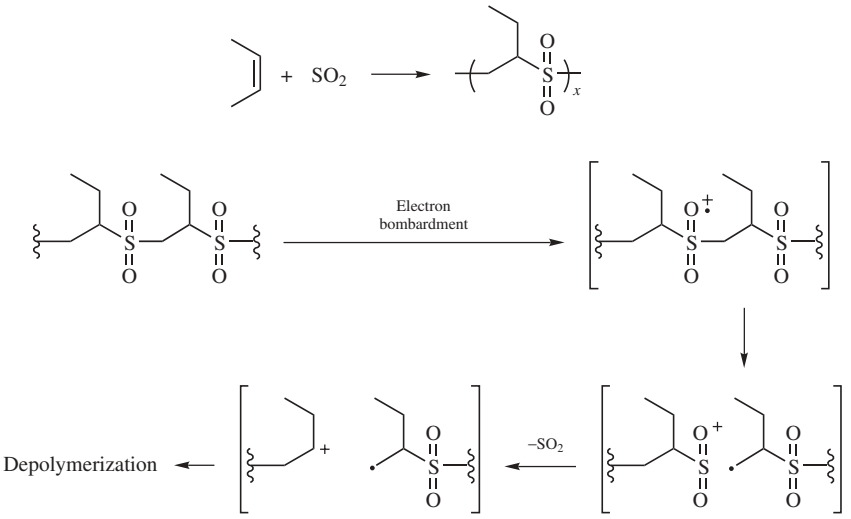

Fig. 4. Chemistry of PBS e-beam resist.

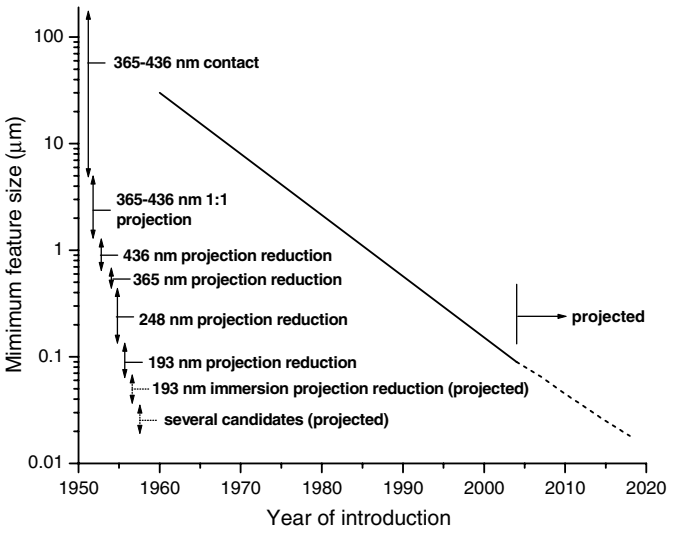

Fig. 5. A graph of the minimum feature size in commercial microelectronic device as a function of the year of introduction. This is one form of Moore's law. The dominant lithographic technology used to produce those devices are overlaid on the plot.

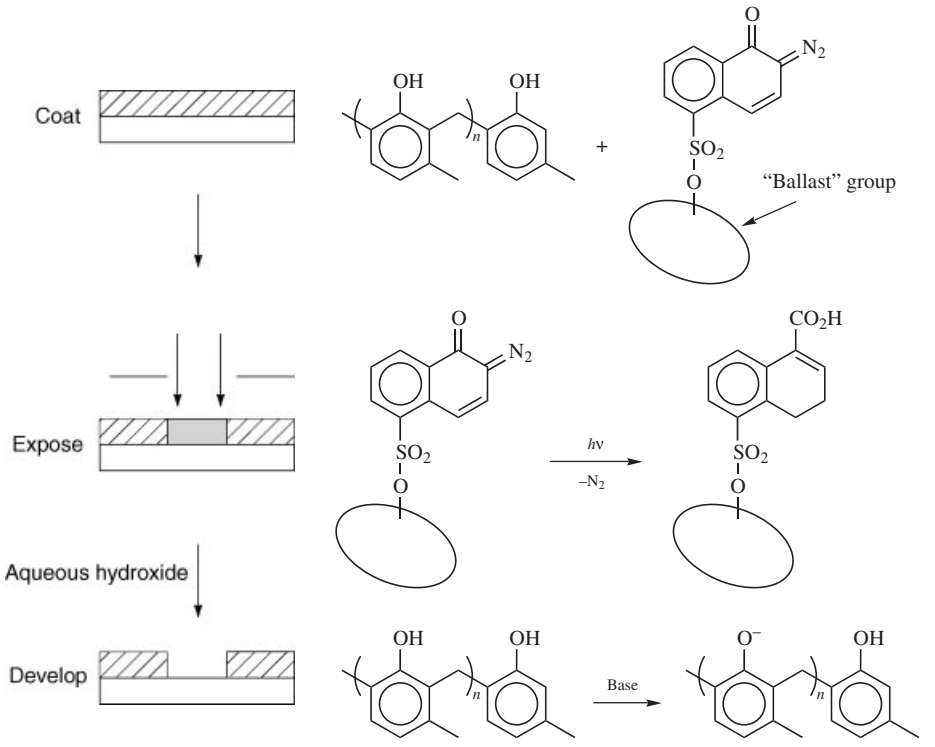

Fig. 6. Chemistry of diazonaphthoquinone–cresol novolac positive-acting resist. During patternwise exposure, the DNQ undergoes photolysis that destroys its inhibitory effect on film dissolution.

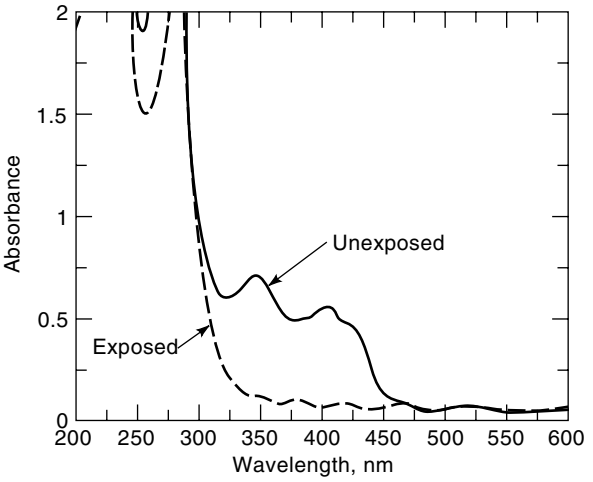

(**a**)

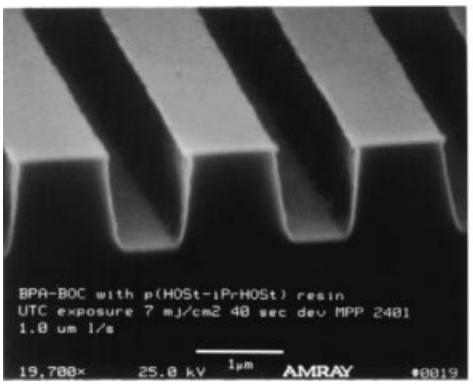

(**b**)

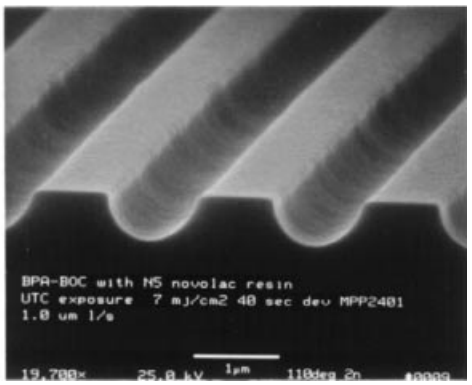

(**c**)

Fig. 7. Influence of optical absorbance on photoresist imaging properties (**a**) The transmittance of a 1-μm film of a typical DNQ–novolac resist after coating is shown as the solid line. The transmittance of the film after exposure with light of 365-nm wavelength. Note the sharp increase in transparency at the exposure wavelength upon exposure, and the high opacity of the film at wavelengths <300 nm; The scanning electron micrographs show relief images obtained using two different photoresist formulations, processed under identical conditions. The formulations are functionally identical but differ in the transparency of the film at the exposing wavelength . (**b**) Image obtained when the film is weakly absorbing (~65% transmittance). (**c**) Image obtained when the film absorbs strongly (<20% transmittance) at the exposing wavelength. Note the incomplete development to substrate and the sloping sidewalls.

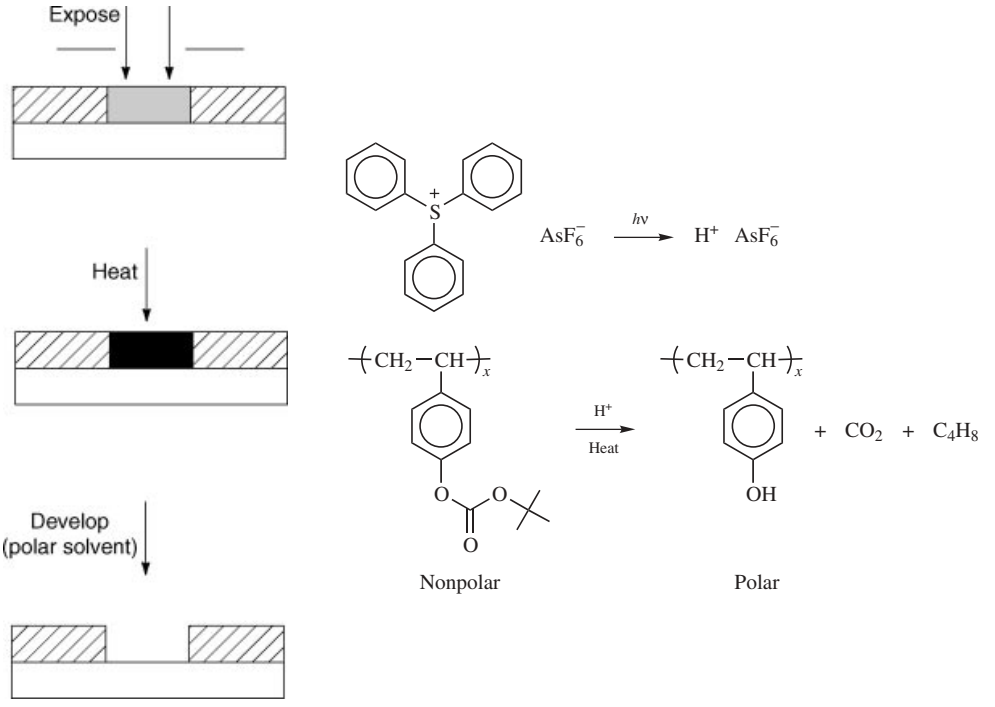

Fig. 8. Chemistry of PTBOCST chemically amplified resist. Patternwise exposure creates small quantities of acid. In a subsequent heating step, pendant TBOC groups are cleaved under acid catalysis. The exposed and unexposed areas can then be differentiated on the basis of solubility.

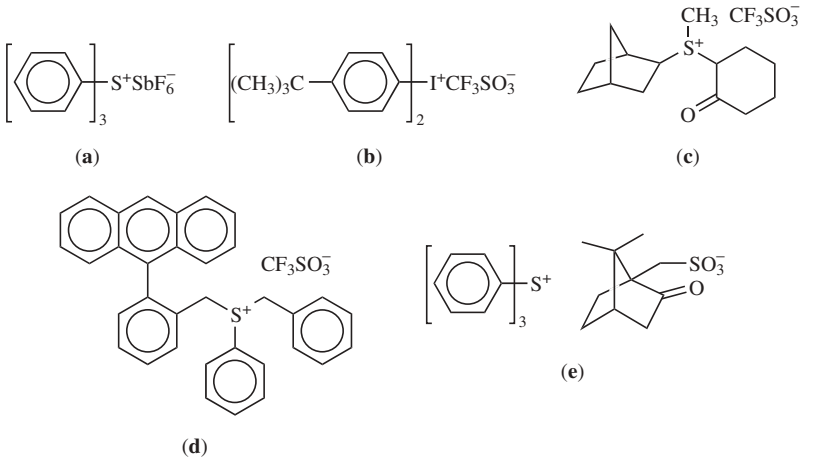

Fig. 9. Structures of selected sulfonium and iodonium salt photoacid generators designed for different lithographic applications. Modifications in the structure of the anion lead to changes in the properties of the photogenerated acid; changes in the structure of the cationic chromophore modify the light absorption properties of the PAG . (**a**) The duv PAG generating inorganic acid; (**b**) duv PAG generating organic acid; (**c**) PAG designed for 193 nm lithography; (**d**) PAG designed for long wavelength activity via intramolecular electron transfer sensitization; and (**e**) PAG designed to generate bulky, weak acid.

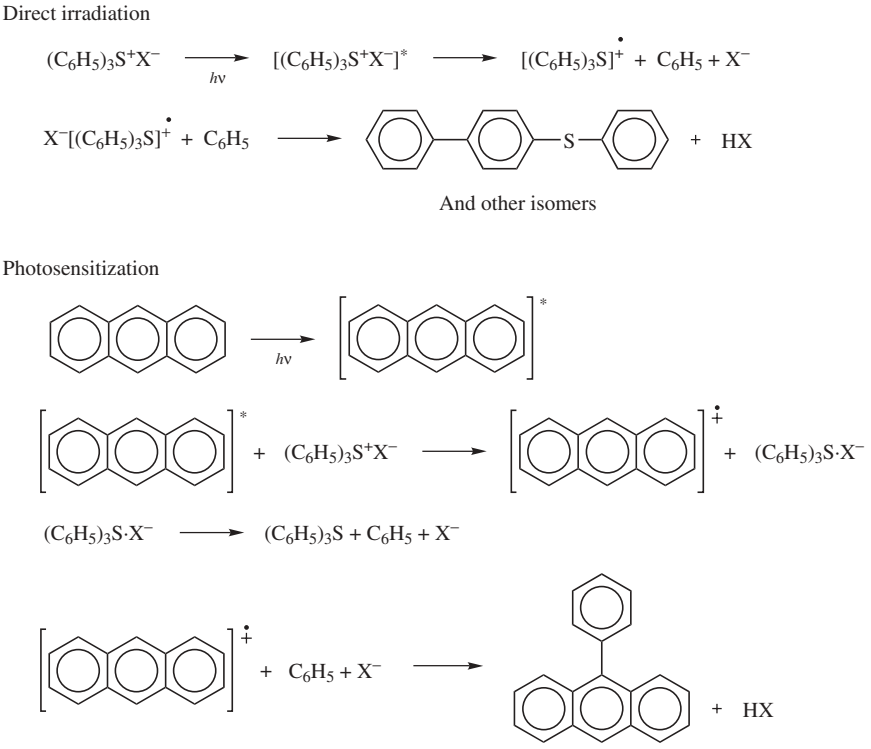

Fig. 10. Proposed photochemical mechanisms for the generation of acid from sulfonium salt photolysis. Shown are examples illustrating photon absorption by the onium salt (direct irradiation) as well as electron-transfer sensitization, initiated by irradiation of an aromatic hydrocarbon.

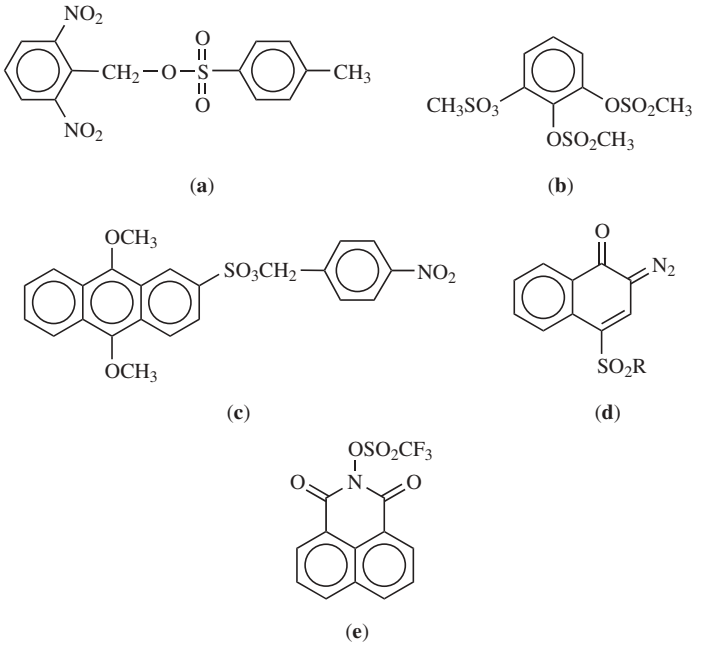

Fig. 11. Representative nonionic photoacid generators. A variety of photochemical mechanisms for acid production are represented. In each case, a sulfonic acid derivative is produced . (**a**) The PAG that generates acid via *O*-nitrobenzyl rearrangement; (**b**) PAG that generates acid via electron transfer with phenolic matrix; (**c**) PAG that is active at long wavelengths via electron-transfer sensitization; (**d**) PAG that generates both carboxylic acid and sulfonic acid; and (**e**) duv PAG generating trifluoromethane sulfonic acid.

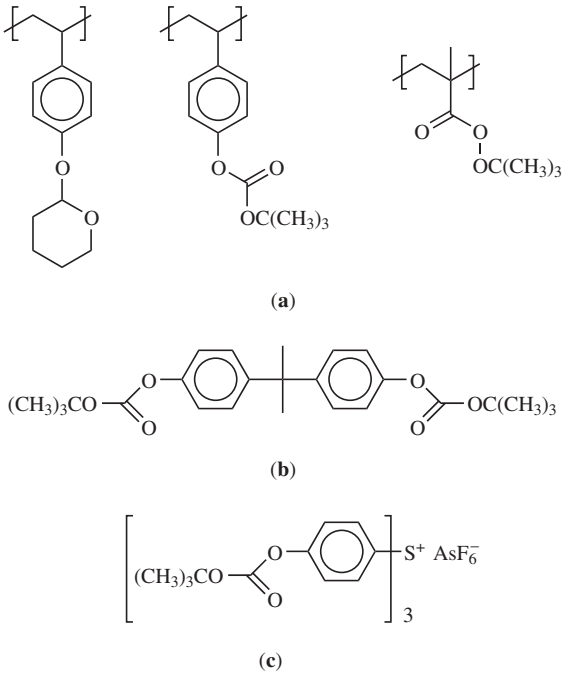

Fig. 12. Representative protecting groups for phenolic and carboxylic acid-based systems. (**a**) The polymer-based protecting groups are listed in order of increasing activation energy for acid-catalyzed deprotection. (**b**) Acid-labile monomeric dissolution inhibitors, a bifunctional system based on protected bisphenol A. (**c**) Another system that combines the function of dissolution inhibitor and PAG in a single unit.

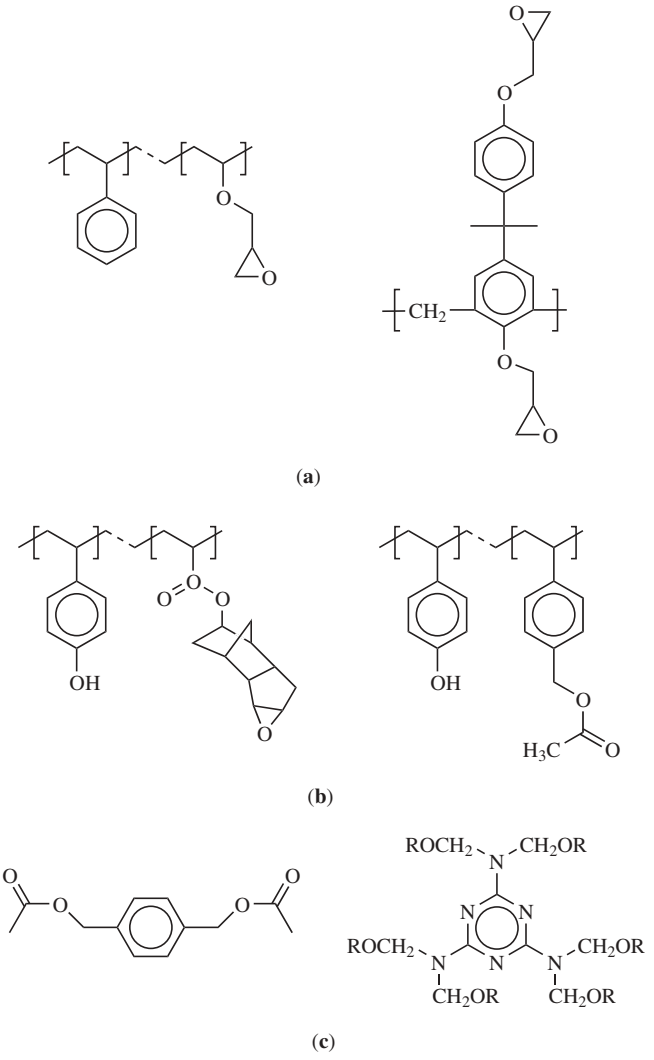

Fig. 13. Representative cross-linking systems employed in negative tone CA resists. (**a**) Epoxy polymers requiring organic solvent development. (**b**) PHOST-based cross-linking systems requiring aqueous development. (**c**) Monomeric cross-linking agents used in PHOST matrix polymers.

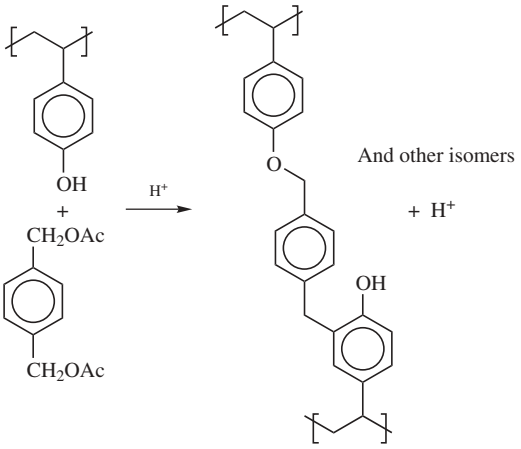

Fig. 14. Cross-linking reactions in a three-component resist system. Both O-alkylation and C-alkylation are shown.

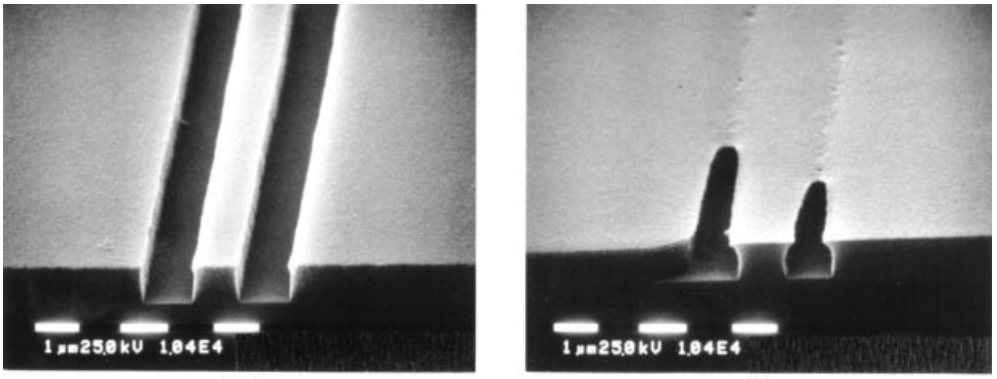

Fig. 15. Scanning electron microscopy (SEM) micrographs illustrating the effects of airborne basic chemical contamination. (**a**) This image was formed when a positive-tone CA resist was processed without any delay after coating. (**b**) This image was formed when an identical film was stored after coating for 15 min in an atmosphere containing 10 parts per billion (ppb) on *N*-methylpyrrolidone, and then processed identically to the first film.

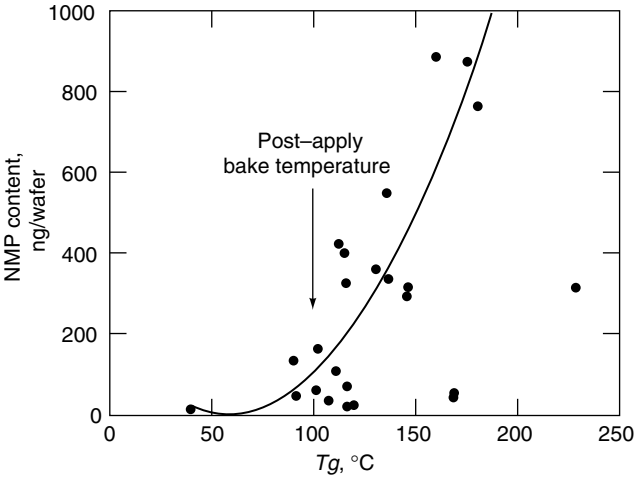

Fig. 16. Correlation of NMP uptake with polymer T_g for a series of 24 different polymeric films. All films were heated after coating at 100°C for 300 s .

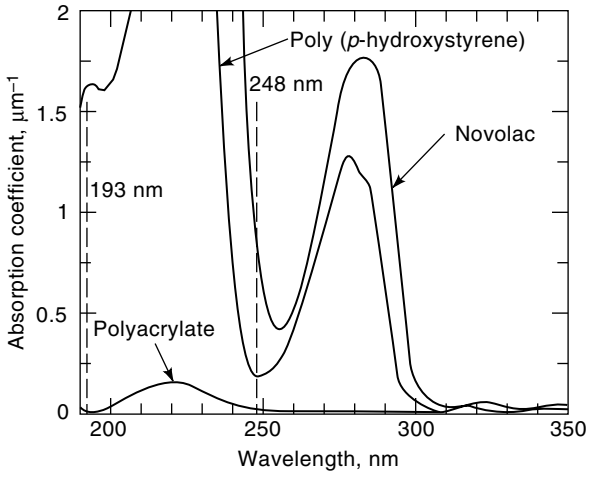

Fig. 17. Optical absorption spectra of 1-μm thick films of novolac, PHOST and polyacrylate polymers. The novolac resin is transparent only > 300 nm. While PHOST also absorbs strongly < 300 nm, it exhibits a region of adequate transparency centered near 248 nm. The acrylate polymer is quite transparent over the uv range.

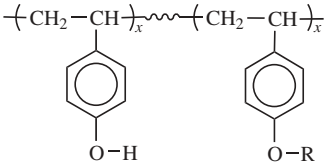

Fig. 18. Traditional duv-resist design using derivatives of PHOST. Monomer (**a**) contributes hydrophilic character to the polymer, and its acidic phenol group enhances aqueous base solubility; monomer (**b**) provides acid-labile pendent groups.

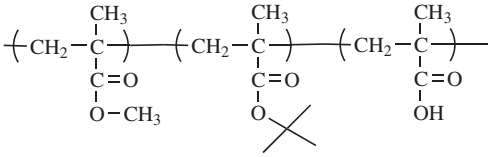

MMA **TBMA** **MAA**

- hydrophilicity
- PAG solubility
- low shrinkage
- adhesion
- mechanical

- acid-catalyzed deperotection

- Aqueous solubility
- increased To

(**a**)

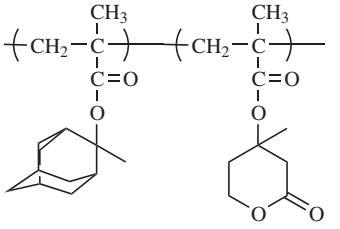

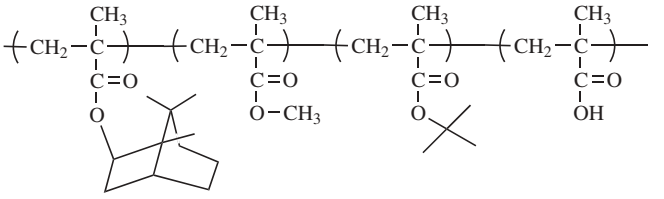

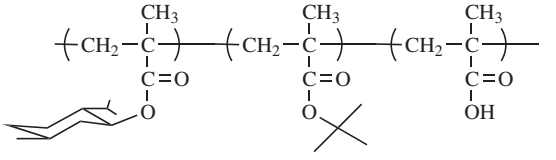

(**b**)

Fig. 19. Candidate acrylic polymers for 193-nm resists. (**a**) A terpolymer designed for chemically amplified resist applications. The properties each monomer contributes to the final polymeric structure are enumerated; (**b-d**) examples of copolymer structures that have been applied in 193-nm CA photoresists. Methylmethacrylate = MMA, *tert*-butyl methacrylate = TBMA, methacrylic acid = MAA.

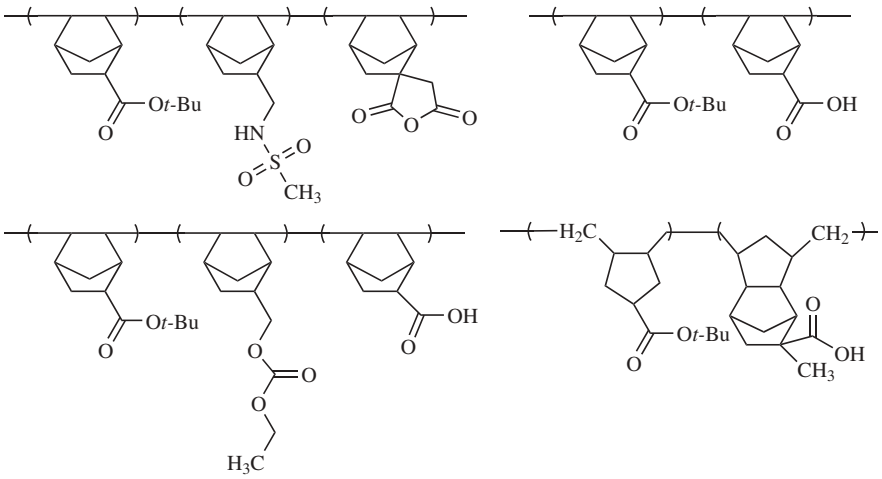

Fig. 20. Cyclic olefin copolymers evaluated for 193-nm resist applications.

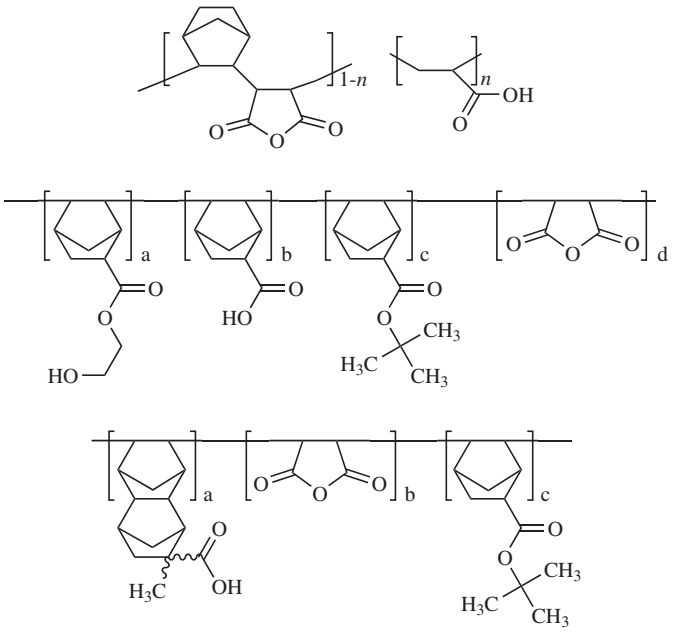

Fig. 21. Cyclic olefin–maleic anhydride copolymers for 193-nm lithographic applications.

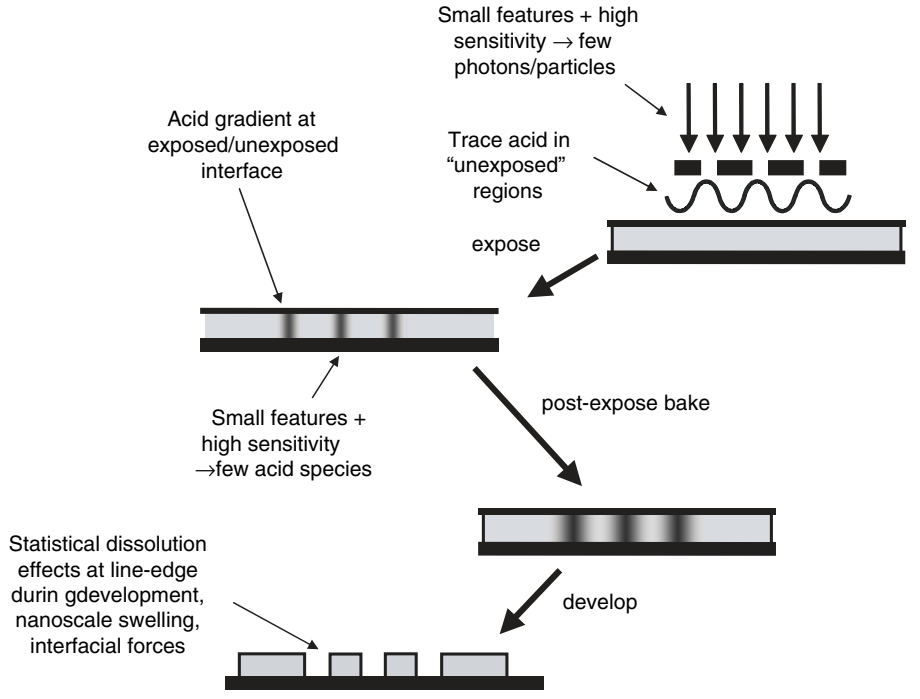

Fig. 22. Origins of limiting factors in CA resists.

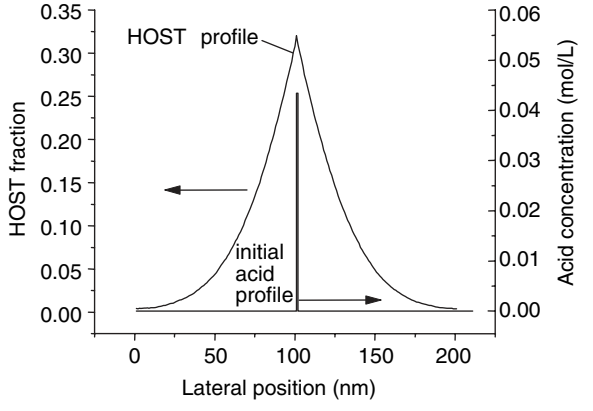

Fig. 23. Plot of the amount of deprotection as a function of position after simulation of the PEB process. An exposure producing a line 1 nm wide is assumed, and the initial acid concencentration is plotted. The broad HOST profile represents the spatial distribution of the deprotection product after the PEB step is complete. This broadening is due to diffusion of the photogenerated acid followed by acid catalyzed deprotection to produce HOST.

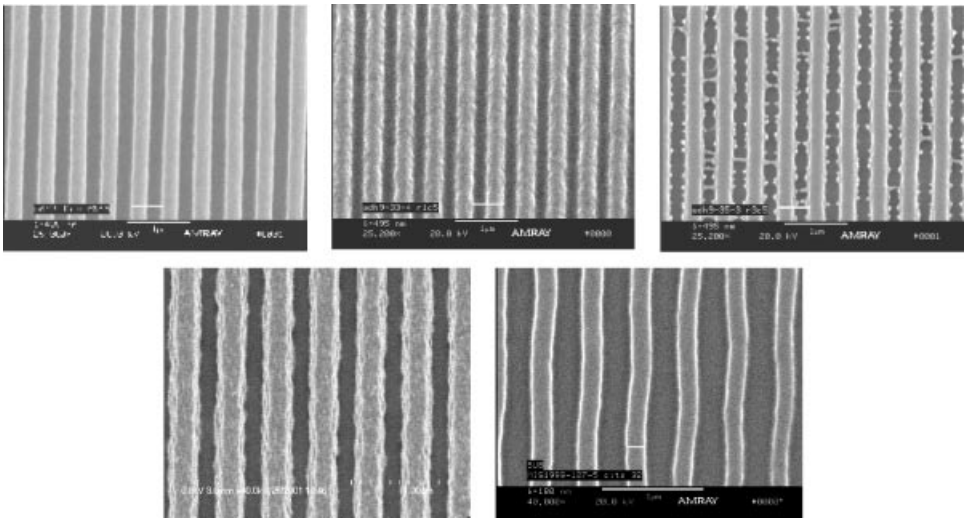

Fig. 24. Top-down SEM micrographs of developed resist images depicting line edge roughness with different characteristics (images courtesy M. Sanchez, IBM Corp).

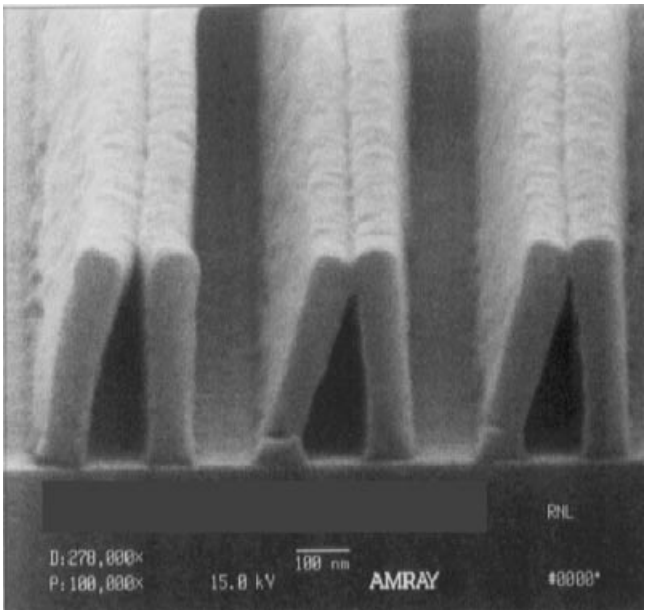

Fig. 25. The SEM of a CA resist pattern illustrating image collapse during postdevelop drying. Note the fracture of the resist structure near its base. (Photograph courtesy D. Medeiros of IBM.)

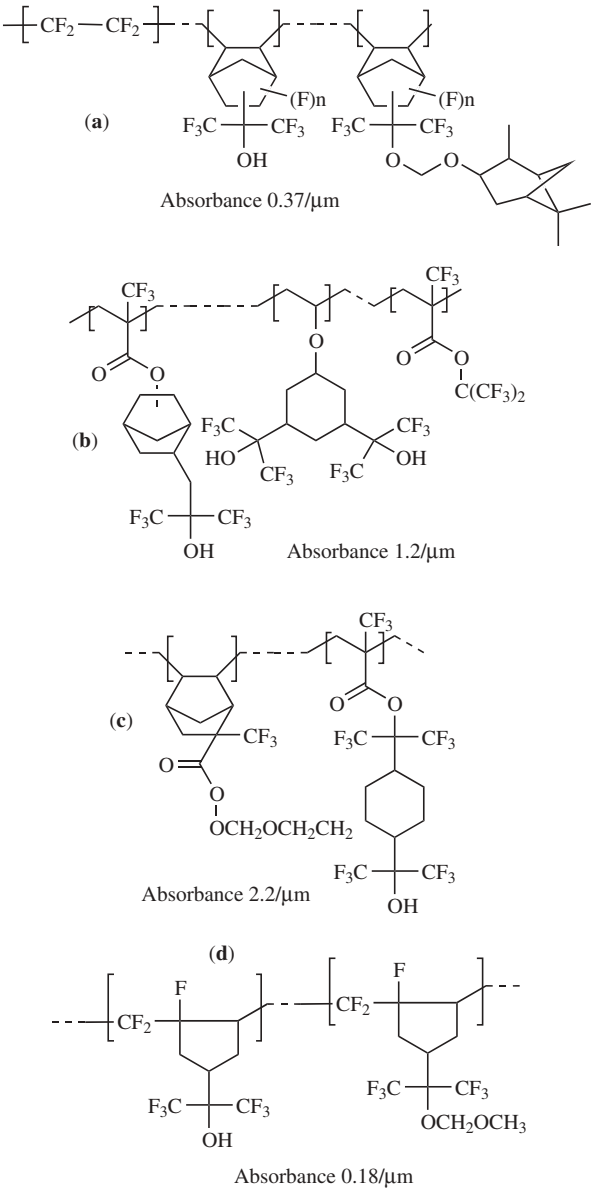

Fig. 26. Examples of polymers used in formulating 157-nm CA photoresists (183–186).

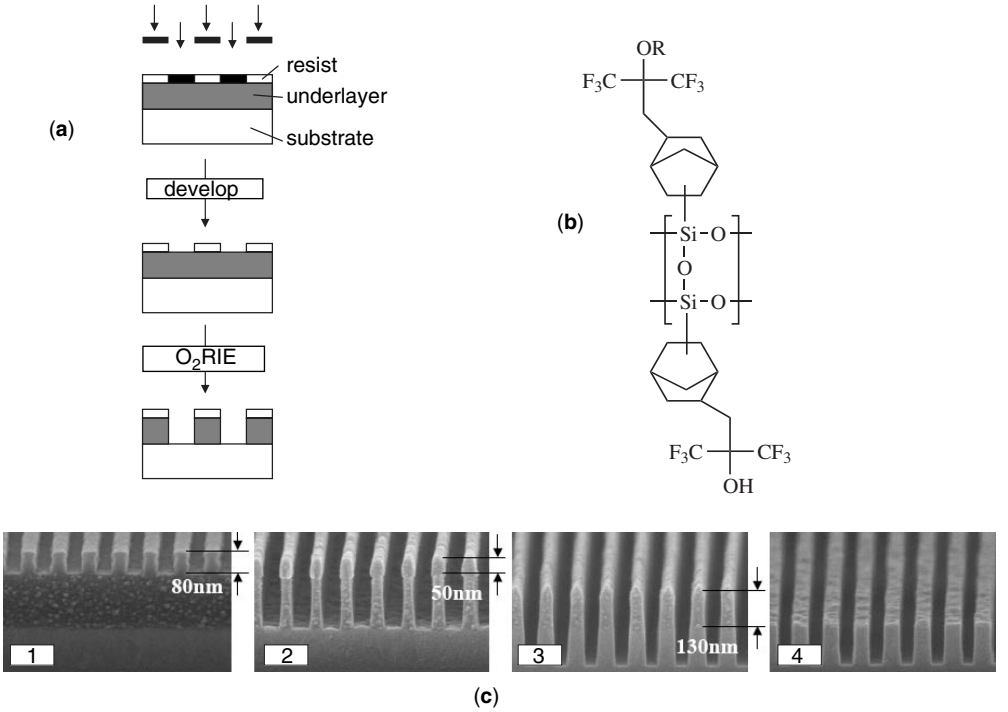

Fig. 27. Multilayer resist process for 157-nm lithography. (**a**) Schematic of a multilayer resist process using a dry etch step to transfer the top image into a thick organic underlayer. (**b**) Generic example of a silicon-containing resist polymer for use as the top imaging layer. (**c**) The SEM micrographs of images formed by (1) 157-nm exposure and development, (2) underlayer etching, (3) substrate etching, and (4) resist removal. (Micrographs courtesy of T. Shimokawa, JSR Corp.)

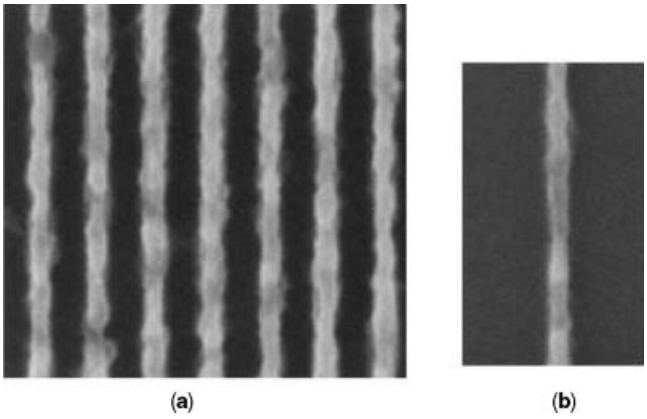

Fig. 28. Images in an experimental resist exposed using euv projection lithography. (**a**) nominal 30-nm nested lines, (**b**) 25-nm isolated line. (Courtesy P. Naulleau, Lawrence Berkeley National Laboratory.)

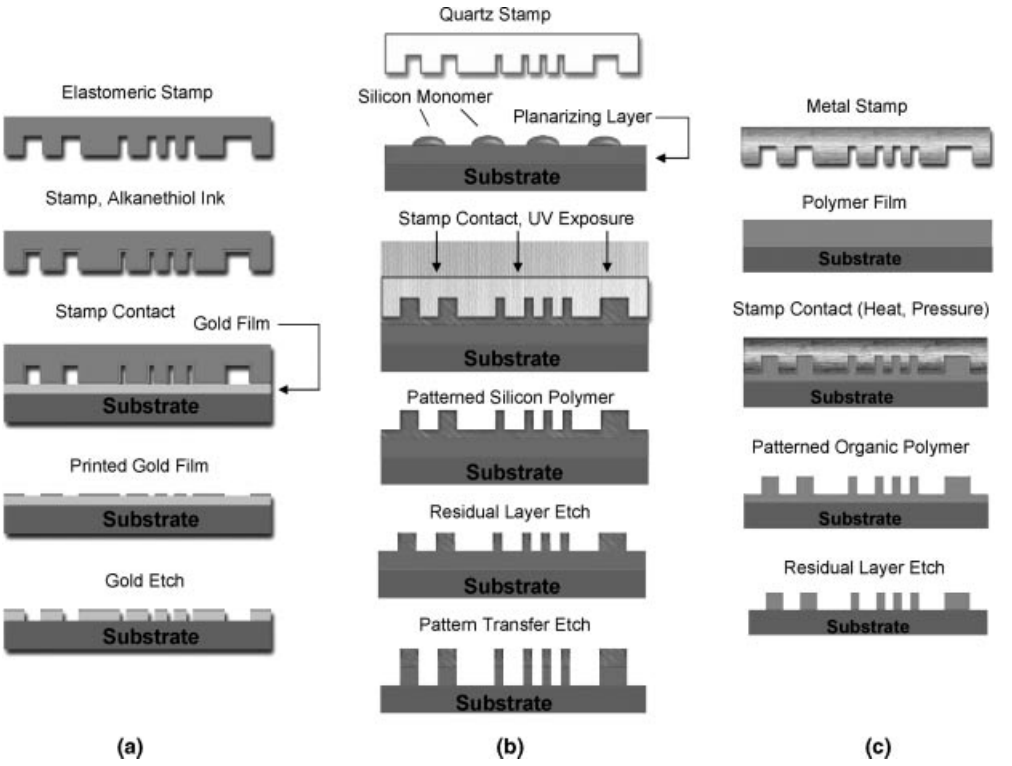

Fig. 29. Lithographic methods that use a direct contact with a template or stamp to form the pattern: (**a**) Microcontact printing, (**b**) nanoembossing, (**c**) optical nanoimprinting.

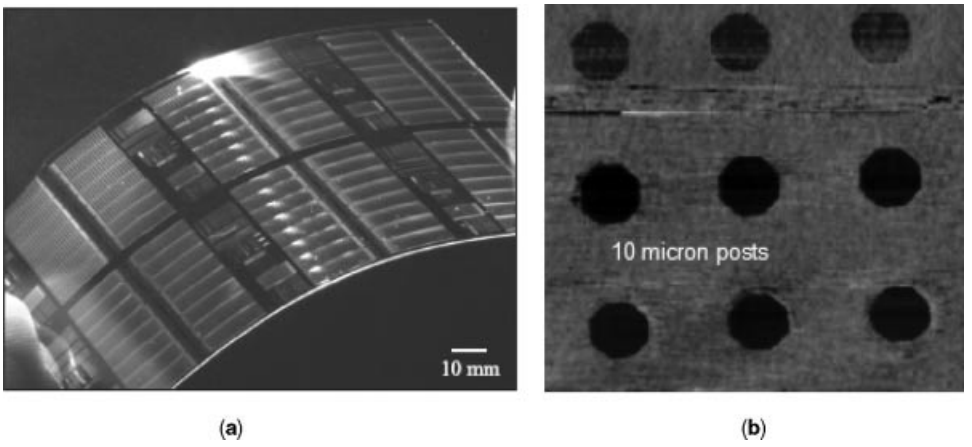

Fig. 30. (**a**) Photograph of an elastomeric stamp (Courtesy B. Michel, IBM); (**b**) atomic force microscopy image of a gold substrate printed with hexadecanethiol (Courtesy J. Frommer, IBM).

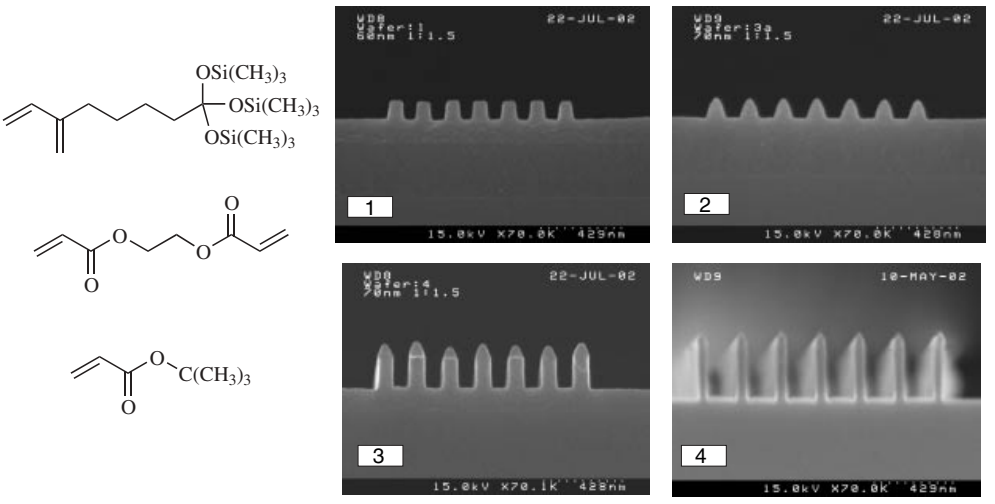

(**a**) (**b**)

Fig. 31. (**a**) Representative examples of acrylate monomers employed in optical nanoimprinting; (**b**) SEM micrographs of images formed at different stages of the optical nanoimprinting process: (1) the imprinted substrate after photopolymerization and mold release, (2) the etched pattern after removal of residual layer, (3) the etched pattern after transfer to the planarizing layer, and (4) the etched substrate after transfer etch. (Photos courtesy C. G. Willson, University of Texas.)